ISSUES PERTAINING TO DIELECTRIC ASSESSMENT OF SOIL MOISTURE IN A COAXIAL CELL

By

JAMES DUVALL

Bachelor of Science in Electrical Engineering

Oklahoma State University

Stillwater, Oklahoma

2007

Submitted to the Faculty of the
Graduate College of the
Oklahoma State University
in partial fulfillment of
the requirements for
the Degree of
MASTER OF SCIENCE
December, 2010

ISSUES PERTAINING TO DIELECTRIC

ASSESSMENT OF SOIL MOISTURE IN A COAXIAL

CELL

Thesis Approved:

Dr. Charles Bunting

Thesis Adviser

Dr. James West

Dr. Paul Weckler

Dr. Mark E. Payton

Dean of the Graduate College

ACKNOWLEDGMENTS

I would like to thank Dr. Charles Bunting for serving as my thesis advisor and helping me through this process. I would also like to thank Dr. Jim West and Dr. Paul Weckler for their guidance and for serving on my thesis committee. Their insights and feedback were essential to the process.

I would also like to thank my friend Clinton Cosgrove for his invaluable assistance and insights, having previously completed a thesis of his own.

I would also like to thank Dr. Alan Cheville for the guidance and expertise he provided.

I'd also like to thank my wonderful parents for their guidance and support and for instilling in me the work ethic needed to complete this project.

TABLE OF CONTENTS

Chapter Page

I. INTRODUCTION 1

II. REVIEW OF LITERATURE 4

2.1 Background on Soil Moisture 4
2.2 How Soil Moisture is Quantized 7
2.3 How Soil Moisture is Changed 8
2.3.1 Soil Moisture Reduction 8
2.3.2 Soil Moisture Increase 9
2.4 Common Measurement Methods 9
2.5 Dielectric Spectroscopy 12
2.5.1 Dielectric Spectroscopy in Agricultural Applications 12
2.5.2 Dielectric Spectroscopy and Soil Moisture 14
2.5.3 Coaxial Cell 14
2.5.3.1 Previous Use 14
2.5.3.2 Weaknesses in Previous Model 16

III. METHODOLOGY 19

3.1 Coaxial Cell 19
3.1.1 How It Works 21
3.1.2 Strengths 22
3.1.3 Weaknesses 22
3.1.4 Treatment of Samples 23
3.1.5 Taking Data 24
3.2 Transmission Line Model 24
3.3 Permittivity Calculation Algorithm 27
3.4 Transmission Line Model 28

Chapter Page

IV. FINDINGS....29

4.0 Load Issues....29
4.1 Teflon Analysis with Load Correction....32
4.2 Distilled Water Analysis with Load Correction....39
4.3 Air Analysis with Load Correction....42
4.4 Comparison of Non-Adjusted to Adjusted Termination Loads....46
4.5 Usefulness of RMSE Analysis....48

V. CONCLUSION....49

5.1 Accomplishments....49
5.2 Future Work....51

REFERENCES....53

APPENDICES....54

LIST OF TABLES

Table Page

1 Soil Moisture Pressure Ranges 5
2 Load Impedances 31
3 Real Reflection Coefficient Analysis of Teflon.....37
4 Imaginary Reflection Coefficient Analysis of Teflon 37
5 Distilled Water Real Reflection Coefficient Analysis.....42
6 Distilled Water Imaginary Reflection Coefficient Analysis.....42
7 Air Sample Real Reflection Coefficient Analysis 46
8 Air Sample Imaginary Reflection Coefficient Analysis 46
9 Comparison of RMSE Measurements for Shorted and Adjusted Loads 47
10 Comparison of Permittivity Estimates for Shorted and Adjusted Loads.....47

LIST OF FIGURES

Figure Page

2.1 Arnold's Coaxial Cell Schematics 15
2.2 Arnold's Transmission Line Model 15
2.3 Arnold's 1 MHz Test Data 17
2.4 Arnold's 100 MHz Test Data 18
3.1 Dimensions of the Coaxial Cell 19
3.2 Coaxial Cell 21
3.3 Transmission Line Model of the Coaxial Cell 25
3.4 Algorithm Flowchart 28
4.1 Teflon Simulation As Load Is Varied 29
4.2 Transmission Line Model With Load 30
4.3 Load Comparison for Distilled Water 31
4.4 Comparison of Real Reflection Coefficient Data and Simulations for Teflon 33
4.5 Magnitude of Error Between Real Reflection Coefficient Data and Sim 34
4.6 Comparison of Imaginary Reflection Coefficient Data and Sim for Teflon 35
4.7 Magnitude of Imaginary Error 36
4.8 Real Root Mean Square Error for Test Relative Permittivity 38
4.9 Imaginary Root Mean Square Error for Test Relative Permittivity 38
4.10 Distilled Water Real Reflection Coefficient Comparison 39
4.11 Distilled Water Imaginary Reflection Coefficient Comparison 40
4.12 Real Reflection RMSE Versus Permittivity for Distilled Water 41
4.13 Imaginary Reflection RMSE Versus Permittivity for Distilled Water 41
4.14 Real Reflection Coefficient of Air 43
4.15 Imaginary Reflection Coefficient of Air 44
4.16 RMSE Analysis of Real Coefficient for Air Sample 45
4.17 RMSE Analysis of Imaginary Coefficient for Air Sample 45

CHAPTER I

INTRODUCTION

The available moisture held within soil is of interest to a wide variety of groups, and many methods have been employed in attempts to analyze it faster and with higher degrees of accuracy. While knowledge of this parameter is highly useful to agricultural and hydrological applications, there are also military and meteorological applications.

Currently, a wide variety of methods are employed to measure soil moisture. Unfortunately, most of these methods are intrusive, time-consuming, and limited in their accuracy. They can also suffer from such issues as requiring the user to handle dangerous materials or only providing data on the very topmost layer of the soil. Many of these problems are further compounded by the fact that soil is not homogeneous, and the moisture content can (and usually will) vary strongly with depth, as well as along a lateral distance from a test point. As such, data collected at a point may be very poorly correlated with other test points that are very close by.

In light of these facts, the need for a fast, portable, non-destructive measurement method of measuring soil moisture is apparent. Such a system could potentially be mounted on a vehicle and used to take data at a great number of sample points which

would be insurmountably time-consuming if attempted with existing destructive on site measurement methods. Such a set of measurements would provide a much better view of the soil moisture content of a field of interest.

Dielectric spectroscopy may provide a platform for a fast, portable, non-invasive measurement method. Before dielectric spectroscopy measurements of soil can be performed on a test field, this method must be successfully applied to a much more controlled environment. In the case of this thesis, a single port coaxial cell was used for its well-known electromagnetic behavior, ability to support a waveguide mode at low frequencies, and because the behavior of the cell will be measured via its reflection characteristics, which is how a non-contact measurement system of soil moisture in a field would be required to operate.

The goals of this thesis are listed as such:

1. Identify the strengths and weaknesses in the previous transmission line model of the coaxial cell.

2. Select and mathematically describe an alternative model to address known weaknesses in the previous model.

3. Produce a simulation tool for the model.

4. Discuss the strengths and weaknesses of the new model.

The rest of the thesis is organized as is described in the following. Chapter 2 is the literature review and contains information on soil moisture, previous measurement methods, and the methods that this study is based on. Chapter 3 describes the methodology which was used to prepare samples, measure samples, and analyze data.

Chapter 4 details the findings of the study and discusses the accuracy of the measurement system. Chapter 4 also discusses the limits of the operating parameters of the system. Chapter 5 is a summary of conclusions that can be drawn from the analysis and recommendations for future work.

CHAPTER II

REVIEW OF LITERATURE

2.1 Background on Soil Moisture

In agriculture, accurate knowledge of the moisture content of a soil sample is a crucial and essential aspect used in making decisions that will, in the end, have a significant impact on crop survival and crop yield. While many factors such as temperature, disease, pests, available nutrients and minerals, and available sunlight play a strong part in whether or not a crop will thrive, available soil moisture is perhaps the most significant factor that can be controlled. For a plant to survive, adequate moisture must be available in the soil in the plant's root zone. The root zone being the range of depth in the soil in which the plant's roots extend. (Donahue, 1977)

Moisture stored in soil is trapped within the pore space of the soil. The amount of suction force holding the water in the pore space determines availability. The following table shows the commonly used ranges for pressure.

Table 1 Soil Moisture Pressure Ranges (Donahue, 1977)

Pressure (Bars)	Comment
< 0	Ground is flooded
0 to 1/3	Gravitational water. Will drain off from the force of gravity alone.
1/3 to 15	Water available to plants.
> 15	Unavailable water. Generally the permanent wilting point.

It is essential to consider that not all soil moisture is moisture that is available to crops. Moisture stored in soil is characterized by the suction force holding it into the pore space. Moisture held with 0 to 1/3 bars of suction is considered to be gravitational water, as the suction force of the pore space is not strong enough to hold onto the moisture stored and gravity will cause it to drain away. The amount of moisture the soil can hold before the suction force falls to 1/3 bars is called the field capacity. The field capacity includes available water and unavailable water but does not include the drainable gravitational water and any standing flood water. (Donahue, 1977)

Available water is moisture that is considered to be available to plants in such a manner that it can be readily absorbed by plant roots to sustain the plant's life. Available water is defined to be moisture that is stored between 1/3 and 15 bars of suction force. In general 15 bars is considered to be the highest suction force for available water as it is the point at which most crops are no longer able to absorb moisture quickly enough from the soil to keep up with the moisture lost from the plant via transpiration. (Donahue, 1977)

Soil moisture stored in the pore space at suction forces greater than 15 bars is considered to be unavailable water. Unavailable water includes all moisture stored below the permanent wilting point of 15 bars. It is also important to note that wilting is not a good indicator of when plants need water because they will have needed water long before wilting occurs. (Donahue, 1977) Because the volumetric water content that corresponds to the aforementioned pressure ranges varies from soil type to soil type, knowledge of the volumetric water content is not enough unto itself to determine how much water is available to crops.

Plant growth will already have been significantly reduced by the time wilting occurs. Wilting can be extremely damaging in a seed crop if a lack of water occurs between the onset of flowering and seed set. (Hanks, 1980)

The suction force described above is not exclusively a function of the volumetric water content. Other features such as the soil's porosity can have a profound effect on the amount of moisture that is in the available suction range for the plants. These attributes vary strongly with soil type, which can vary strongly with distance in a given field of soil. As such, it is difficult to make a good estimation of how much water is available to plants without the volumetric water content as well as the soil's available water profile. (Donahue, 1977)

There are four regions used to define how full the pore space is in soil. The first, least filled region, is the pendular region. In this region, only water vapor is present in the

pore space. Next is the funicular stage. In this region the pores are filmed with liquid. Beyond that is the capillary stage, in which all of the pores are filled with water. Finally, on the opposite extreme end, is the phrentic stage. The phrentic stage is used to describe soil beneath the level of the water table. (Gelalecha, 2000)

Water content in soil can have sharp discontinuities across distance. Discontinuities occur primarily at a drying front or wetting front, which occurs whenever there is a sharp boundary between two soil types. In situations such as these, a single point measurement of soil moisture could prove to be disastrous for plants attempting to grow on the other side of such a boundary.

2.2 How Soil Moisture Is Quantized

The amount of soil moisture present in a sample can be quantized in three ways. These are: a volumetric basis which is a ratio of the volume of water present to the volume of soil present, a dry mass basis which is a ratio of the mass of water present to the mass of soil solids present, and a wet mass basis which is a ratio of the mass of water present to the sum wet soil. (Hanks, 1980)

Mass Water Content Formula (Wet Mass):

$$\theta_W = \frac{MassWater}{MassWetSoil} \tag{1}$$

Mass Water Content Formula (Dry Mass):

$$\theta_m = \frac{MassWater}{MassDrySoil} \quad (2)$$

Volume Water Content Formula:

$$\theta_V = \frac{VolumeWater}{BulkVolumeSoil} \quad (3)$$

2.3 How Soil Moisture Is Changed

Soil moisture levels change easily and often. As a result, it is necessary to measure moisture frequently to maintain accuracy. The number of different effects which cause moisture levels to increase or decrease significantly complicates any attempt to estimate change over time without a direct measurement. The time-dependent fluctuation in moisture content calls into question the usefulness of any measurement method which requires a long time to process or gather data.

2.3.1 Soil Moisture Reduction

Evapotranspiration is the cycle in which moisture is released from a field via evaporation and transpiration of water from the soil and crop. Evapotranspiration can be measured with a lysimeter (discussed in detail and section 2.4), which is essentially a large soil tank that measures the weight of the crop and its soil.(Hanks, 1980) (Donahue, 1977) Lysimeters also operate under the premise that any change in the weight in the tank can be attributed to water.

In addition to evapotranspiration, soil moisture is also reduced by drainage of gravitational water. Gravitational water includes any amount of water that is stored in the pore space at under 0.5 bars of suction pressure, previously referred to as gravitational water in section 2.2, which will eventually drain away from gravitational forces. (Donahue, 1977)

2.3.2 Soil Moisture Increase

Soil moisture levels are generally increased by two phenomena: precipitation and irrigation. Often precipitation is not a sufficient source of water to sustain a crop. The insufficiency is due primarily to the significant amount of water lost through transpiration through the crops themselves. Gravitational run off is also a contributing factor, but studies have shown that transpiration and evaporation are the most significant factors by a very wide margin. (Hanks, 1980)

2.4 Common Measurement Methods

In the past, many methods of measuring soil moisture have been employed, all of which require a significant time and/or monetary investment. Perhaps the most basic method of calculating soil moisture is to sample the soil in question and measure the mass of the soil when wet and once it has dried. This method is advantageous as it requires very little equipment and no significant training. This method is, however, extremely time consuming as the soil sample must be collected, removed to a testing area, measured, and then very thoroughly dried before the dry mass is measured. This method is also disadvantageous in that the sample only represents the soil moisture in one

very small region and the results often do not reflect the present condition of the soil by the time they can be calculated. The process is also significantly destructive because the soil must be removed from the ground in order to be measured.

An alternate method to the basic practice described above includes the use of blocks of gypsum or other porous materials. These porous blocks are measured by digging holes at the desired measurement site and burying them at various depths in the root zone. The blocks are then read by measuring the electrical resistance with the knowledge that as the moisture level decreases the electrical resistance of the block will decrease. (Donahue, 1977) Before burial each of the blocks must be thoroughly soaked, dried, and soaked again in order to free any trapped air. The blocks must then be carefully buried such that all of the soil in the hole is tightly packed. Ideally the pore space of the soil replaced into the hole should be identical to that of the surrounding soil. Most essential, however, is ensuring that there is not a loose soil path connecting the soil surface to the sensor blocks. If this occurs the moisture reading will be wildly inaccurate due to the loose soil connection's ability to hold significantly more moisture than the soil surrounding it. This method is favorable in that it is inexpensive.

One can easily see that the method only provides a very localized measurement. One can also see that, due to the care needed in the installation process, installation of multiple probes can quickly become very time consuming as well as very expensive. Additionally, there is inherent inaccuracy in the system due to the pore space in the installation hole being unequal to the pore space of the surrounding soil. The blocks are

also known to deteriorate significantly when installed in soil and thus produce less accurate results the longer they are exposed to the soil and water. One can also see how an installation error could go undetected and without additional sensors to check against, inaccurate data could prove disastrous for moisture maintenance leading to low crop yield or crop failure.

Lysimeters are also employed to measure soil moisture. A lysimeter is essentially a soil tank that contains soil and any crop growing in it. The tank is connected to a scale, and available moisture is calculated by monitoring fluctuation in weight. The tank's measurements are of limited accuracy because it can only be placed in one location. An important weakness to consider in a lysimeter is its inability to account for water stored in the pore space at under 0.5 bars, which would normally run off due to gravitational forces, but in this case would remain trapped within the tank. Lysimeters must also be very carefully placed, as the terrain can play an important impact how water flows across the field during periods of precipitation or irrigation. Positions at high points in the field will generally suffer from lower water received and lower points will generally have higher amounts. Either of these conditions can make the lysimeter produce a measurement that is not characteristic of the rest of the field. (Donahue, 1977)

Tensiometers have also been employed to measure soil moisture. These devices measure the attractive forces between water and soil particles, effectively measuring the difficulty plants will have in drawing water from the soil. The disadvantage to using a tensiometer is only one location is measured and the accuracy of the devices decays with time as air leaks into its system. The devices also suffer from a strong dependence on temperature and air pressure which can easily exacerbate the previously mentioned issue

of air leaking into the system.(Arnold, 1992) Tensiometers also suffer in their effectiveness as they are only effective from 0 to 0.85 bars of pressure. This range is mostly in the gravitational run off range. It does not come remotely close to reaching the 15 bars pressure of wilting point or even extend significantly deep into the available water range. However, tensiometers may be applied more readily in sandy soils, where the available water is stored at a lower pressure range. (Donahue, 1977)

2.5 Dielectric Spectroscopy

2.5.1 Dielectric Spectroscopy in Agricultural Applications

Of the methods currently employed to measure soil moisture levels, Dielectric Spectroscopy offers the most expedient form of measurement and provides a measurement platform which has the potential for a highly mobile measurement system for quick, accurate in situ measurements. In agriculture, proper management of moisture available to crops is essential in guaranteeing the survival and health of a crop. Dielectric spectroscopy is a safe, non-destructive method for measuring soil moisture. Of current methods, dielectric spectroscopy and other non-destructive microwave analysis techniques are noteworthy in that they do not rely on contact with the soil to measure its moisture content.

Other methods of soil moisture assessment rely heavily on contact with the soil sample and can require excavation or other complicated installation processes. These methods also often involve lengthy testing periods: requiring porous blocks to gain equilibrium with the soil surrounding them, requiring soil to be given time to dry, or

requiring a device to equalize its pressure with the tension forces in the soil sample itself. All of the downsides of these common methods are well-documented and widely known, yet they are still employed because of a lack of an affordable, viable alternative.

Many papers have been written detailing the benefits and disadvantages to soil moisture measurement with Time Domain Reflectometry (TDR) or Dielectric Spectroscopy. (Gelalecha, 2000) (Topp et. al., 1980) (Rial, 2001) (Nelson, 2005) (Nelson, 1991) (Jorgensen 1970) (Trabelsi 2010) The results of these experiments have been largely successful. An experiment was conducted using a probe to determine the volumetric water content of soil using the apparent dielectric constant. This experiment operated under the ideal condition of a completely homogenous soil consisting of 85% sand and 15% pulverized peat moss. The high sand content encouraged rapid draining to expedite experimental procedures. This experiment yielded positive results with a strong correlation between the volumetric water content calculated by the probe and the actual measured water content (W.S. Rial, 2000). Another experiment was conducted using a frequency response sensor over a range of frequencies from 200 Hz to 100 MHz. The experiment investigated soils of various textures, densities, salinities, and water content levels. This study found that soil moisture and soil salinity could be measured by the magnitude ratio and the phase shift of their frequency response (Lee, et. al, 2007). A study was conducted to measure the scattering parameters of several soils of different mineralogies as a function of frequency and soil moisture. Samples were tested in a truncated coaxial cell with a Vector Network Analyzer. This experiment showed that in highly saline soils, relaxation frequencies can complicate the data (Logsdon, 2005). Other

experiments have also been conducted using dielectric spectroscopy in a number of agricultural applications. These include soil moisture, insect presence, quality of grains, densities of products, quality of oilseed crops, and quality of peanuts.

2.5.2 Dielectric Spectroscopy and Soil Moisture

Another method of measurement that is being investigated employs time domain reflectometry to measure the apparent dielectric constant (the complex dielectric constant) of the soil medium. It has been found that the apparent dielectric constant of soil varies strongly with the volumetric water level and very weakly with the soil's density, texture, salt content, and is insensitive to temperature.(Gelalecha, 2000) (Rial, 2001) This overcomes several of the most common obstacles to measuring soil moisture; obstacles such as sensitivity to air pressure, temperature, and salt content in the soil, amongst other things. Using time domain reflectometry to measure the apparent dielectric constant of a soil medium confers an additional benefit to the procedure. The measurement device does not have to be in contact with the soil. This allows for a highly mobile sensor apparatus which can take and process measurements very quickly which is well in line with the goal of creating an expedient measurement system. (Lee, 2007)

2.5.3 Coaxial Cell

2.5.3.1 Previous Use

The coaxial cell (seen in figure 2.1) was previously constructed in a study by Arnold. Arnold's study used a transmission line model to characterize the behavior of the cell. This model is shown below in figure 2.2.

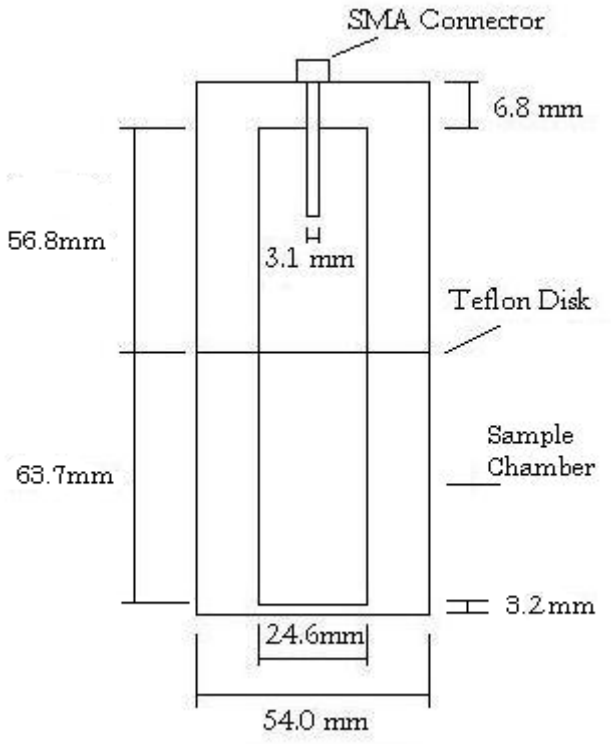

Figure 2.1 Arnold's Coaxial Cell Schematics

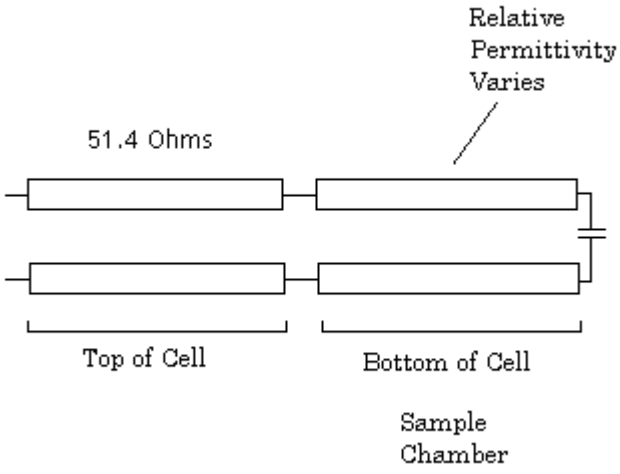

Figure 2.2. Arnold's Transmission Line Model

In Arnold's model, the cell is presented as two transmission line segments. The first represents the top half of the cell, the second represents the bottom of the cell, and the base of the cell is represented with a capacitor due to the capacitance resulting from a

3.2 mm gap between the bottom of the cell and the center conductor. Arnold's method involved calculating the electrical length of the cell from a measured impedance, then numerically solving for the complex propagation constant. The complex propagation constant was then used to calculate the relative permittivity of the sample. Free space permeability was assumed. His study found that accuracy of the relative permittivity calculation improved at higher test frequencies. (Arnold 1990)

2.5.3.2 Weaknesses in Previous Model

Comparison of the physical structure of the coaxial cell (figure 2.1) to the transmission line model (figure 2.2) reveals that several attributes of the coaxial cell's structure are not being accounted for in the transmission line model. The work done in Arnold's study shows a very broad range of permittivity estimations for samples of similar volumetric water content. These ranges are large enough that at lower frequencies, some samples are estimated as having half the relative permittivity of samples with lower volumetric water content. (Arnold, 1990) Since the issue is frequency dependent, lessening in severity at higher frequencies, it seems reasonable to assert that some frequency dependent feature of the coaxial cell is not being properly modeled, causing the measured impedance values to produce a wide range of relative permittivity estimations. Figure 2.3 and 2.4 show Arnold's data for a 1MHz test and a 100 MHz test respectively. Measurements were taken from an assortment of samples. Note in figure 2.3 how widely spread the points are for similar volumetric moisture content ratios. Errors are very significant and apparent in the data. Particularly in the 0.30 to 0.35 range one can observe that samples of similar volumetric moisture content were measured to have relative permittivity values ranging from around 25 to as high as almost 70. The data also

reflects such features as volumetric water content ratios of around 0.30 exhibiting a lower relative permittivity than samples at around 0.20 and similar relative permittivity to samples around 0.10. The wide range of estimations is an undesirable behavior which clearly demonstrates a poor ability to estimate the relative permittivity of the tested samples at this frequency. (Arnold, 1990)

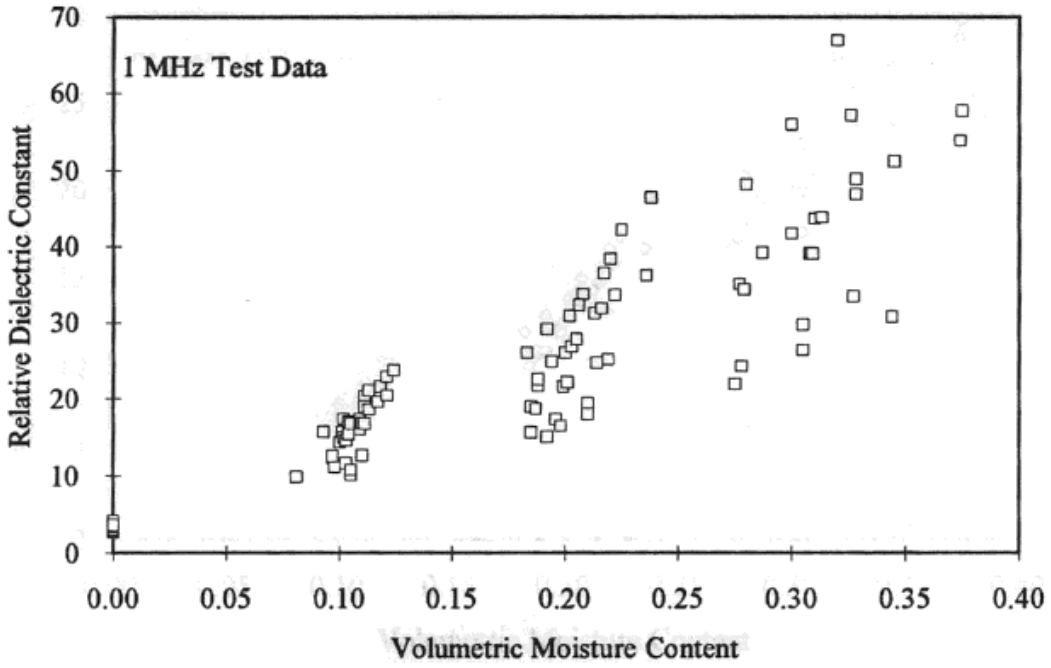

Figure 2.3. Arnold's 1 MHz Test Data (Arnold, 1990)

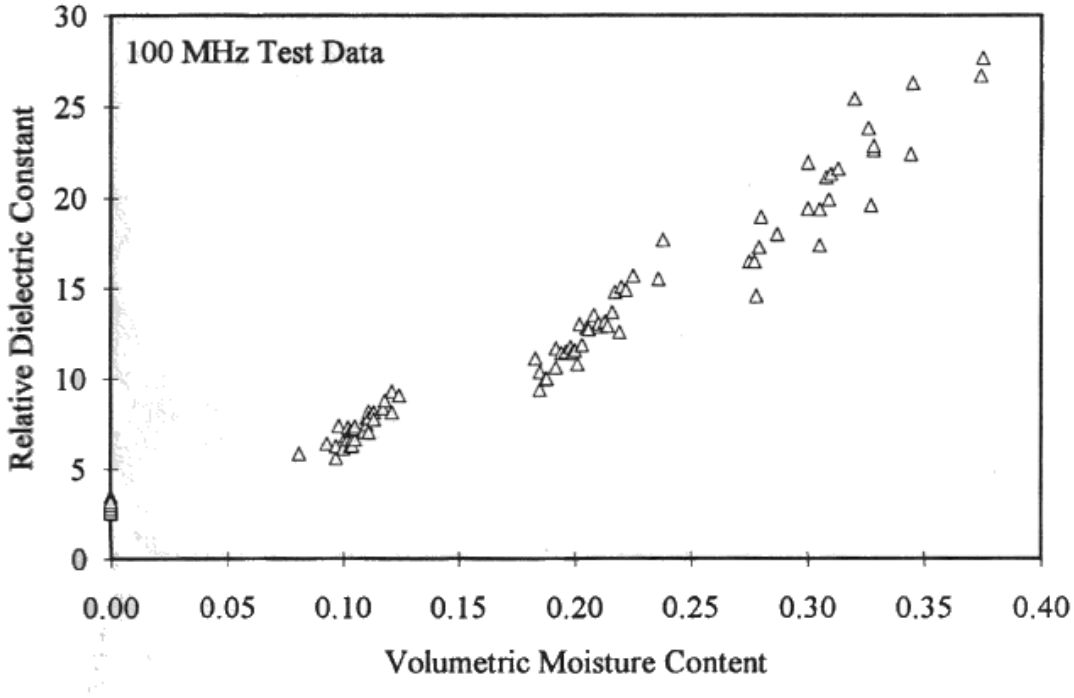

Figure 2.4. Arnold's 100 MHz Test Data (Arnold, 1990)

Figure 2.4 shows Arnold's 100 MHz test data. The spreading issue is less significant here but is still present. The issue is most clearly evident when comparing data gathered at approximately 0.28 volumetric water content to data gathered for about 0.24 volumetric water content. Here, one can see that a sample with 0.28 volumetric moisture content was estimated to have a relative permittivity of less than 15. However, at a lower volumetric moisture content of approximately 0.24, a higher relative permittivity of 18 is measured.

CHAPTER III

METHODOLOGY

3.1 Coaxial Cell

The coaxial cell is a measurement tool capable of measuring the dielectric properties of an inserted material when used in conjunction with a Vector Network Analyzer (VNA). A schematic showing the coaxial cell's dimensions are show in figure 3.1 below. Note that unlike figure 2.1, this schematic shows the center conductor shorted to the bottom plate of the cell. The cell is made of brass and has been silver plated to improve surface conductivity. The center ring is a thin Teflon disk used to regulate the size of the sample. The cell was constructed based on a design used in an earlier experiment in which a coaxial cell was used with dielectric spectroscopy to evaluate the dielectric properties of grains and seeds. (Jorgensen 1970). That experiment used air samples and benzene samples to evaluate the accuracy of measurements taken with the cell. The difference between the modern cell and the cell used in Jorgensen's experiment is the modern cell has no capacitive material added in the connection between the SMA connector and the center conductor. The modern cell's center conductor is shorted to the bottom of the cell, where a small air gap was left in the previous design. Figure 3.2 is a digital photograph of the coaxial cell fully assembled.

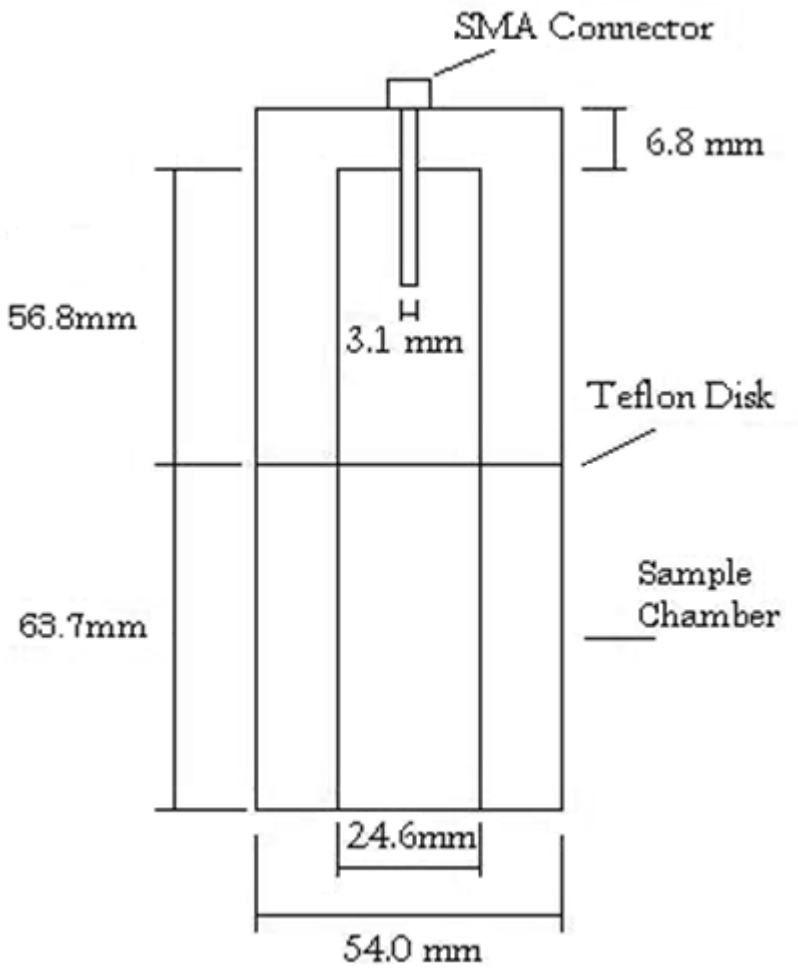

Figure 3.1: Dimensions of the Coaxial Cell

Figure 3.2: Coaxial Cell

3.1.1 How It Works

The coaxial cell has a single compartment for samples. In this thesis, this compartment will be referred to as the sample compartment, and is the bottom half of the cell. For completely solid samples, such as the Teflon insert, the bottom cap may be removed and the insert pressed inside. For liquid samples, only the base of the sample compartment is water tight. As a result, to test a liquid sample, the top half of the cell and the center insert should be removed. Liquid test material could then be poured into the bottom section of the cell. Once a sample is in place, a properly calibrated VNA can be connected to the SMA connector on top of the cell.

3.1.2 Strengths

The coaxial cell is a well-defined structure that has been used in a number of experimental procedures, several of which were discussed in chapter 2. As a result, it is mathematically well-defined. The nature of such a transmission structure lends itself toward measurements of dielectric properties. Additionally, by using only the bottom of the cell to contain the sample under test, the sample compartment is reduced to a very simple geometry. This reduces the mathematical complexity of the design. The chance that a sample will be improperly loaded into the cell is greatly reduced as well.

3.1.3 Weaknesses

The coaxial cell suffers from several weaknesses. First, the conductive center rod does not connect directly to the bottom lid of the sample compartment. As a result, there is a gap between the center conductor's bottom face, and the interior face of the lid which acts as a parallel plate capacitor. The presence of the gap is undesirable because the impedance of the capacitance will vary with operating frequency and cannot be easily calibrated out as a result. Additionally, for granular samples, such as soil, it is difficult to keep the sample from leaking into the gap, altering the permittivity between the plates which is tied directly to the capacitance. Solid samples are easier to keep out of the gap, but the inserted material will still occupy the fringe field of the capacitor and affect its performance. Since the objective is to measure the permittivity and this effect creates a second change in the measurement based on permittivity, it is highly undesirable.

An additional weakness that the cell suffered from was the abrupt change in the diameter of the inner conductor in the top section of the cell. An abrupt change such as

this excites an infinite number of waveguide modes across the discontinuity. These all died out quickly, but produced a capacitance that had to be accounted for in the transmission line model. This capacitance will be discussed in greater detail in section 3.2. Often, a gradual, cone-shaped top is used for the center conductor in similar coaxial cells to greatly attenuate this effect.

3.1.4 Treatment of Samples

Samples consisted of liquid solutions and solid inserts. Soil/water mixtures could also be supported but were not tested. Solid samples were cut to fit snugly into the sample compartment. Liquid samples were poured into the sample compartment through the top under a fume hood. Soil samples should be weighed before being placed into the cell. After measurements, samples must be thoroughly dried and weighed again. The soil sample's particle density should then be measured. This calculation allows for the volume water content to be calculated directly for validation against the coaxial cell's measurement.

Actual samples tested included distilled water, air (empty sample cell), and Teflon. To show that varying water levels in soil produced a varying relative permittivity, several soil samples were also prepared and evaluated. A discussion of these results is presented in chapter 4.

3.1.5 Taking Data

Data was collected by using an Agilent Vector Network Analyzer (hereafter referred to as VNA). The VNA was calibrated for a single port, S11 measurement from 50 MHz to 400 MHz. Short, Open, and Broadband Load calibration standards were used in a kit designated for SMA connectors. 201 data points were taken for each plot. The real and imaginary reflection coefficients as well as the phase and magnitude plots were then recorded for analysis in MatLAB. Data was taken at room temperature.

3.2 Transmission Line Model

In order to simulate the electrical properties of the coaxial cell, a new transmission line model was developed. The model allows for each length of the cell to be broken down into a finite electrical component, assuming that the cell is operating as a transmission line. The final model is pictured below in figure 3.3. Comparing to figure 2.2, one can see that significant changes have been made. The load capacitance has been replaced with a short. This was achieved by compressing a copper mesh tightly in the gap between the center conductor and the bottom plate. Additionally, two admittances in the form of two shunt susceptances are added at the top of the cell to account for the change in the radius of first the outer, then the inner conductor. Between the two admittances, a short transmission line segment has also been added to account for the previously ignored top segment.

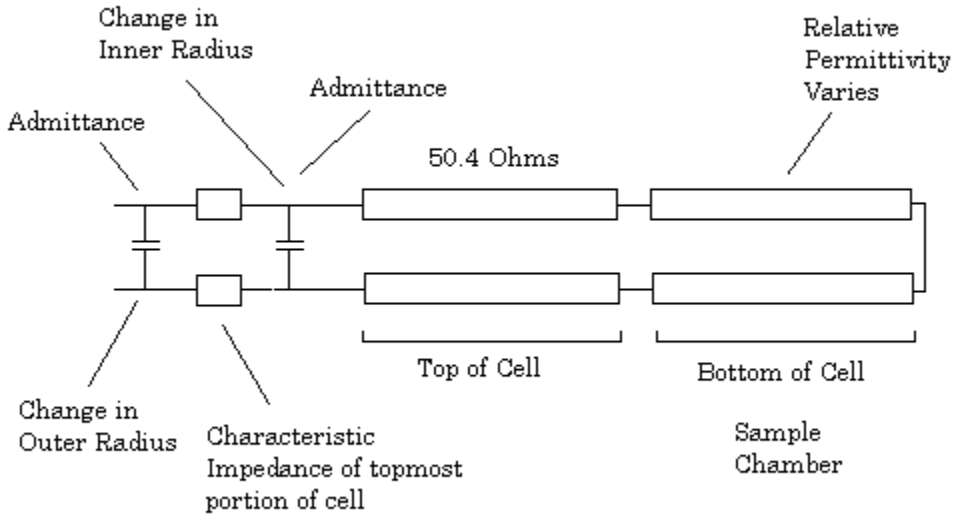

Figure 3.3. Transmission Line Model of the Coaxial Cell

A MatLab program was constructed using the concept of a cascaded transmission line model to simulate the behavior of the cell. Lengths of the cell were treated as transmission line segments with the characteristic impedance calculated by the physical dimensions of the cell, assuming the behavior of a coaxial transmission line. The gap between the internal surface of the sample compartment's bottom lid and the center conductor was modeled as a capacitance load before it was removed via shorting the center conductor to the bottom lid. This capacitance was calculated to be 1.89 pF for the case that air was present between the two panels and neglecting of fringing effects. The two step discontinuities in first the outer conductor and then the inner conductor create a structure that must be modeled as a capacitance in parallel with the susceptance of the sum total of the elements in the transmission line model that occur beyond the discontinuities. Using the characteristic impedances of each section of the transmission line model, input impedances were calculated. The equation below shows the impedance

formula for the sample chamber. It should be noted that because the load for this section is a short circuit, the equation reduces in this segment to the simpler equation seen directly beneath it.

$$Z_i = Z_o \frac{Z_L + Z_o \tanh(\gamma\lambda)}{Z_o + Z_L \tanh(\gamma\lambda)} \quad (4)$$

$$Z_i = Z_o \tanh(\gamma\lambda) \quad (5)$$

$$\gamma = \sqrt{(j\omega\mu(\sigma + j\omega\varepsilon_r\varepsilon_o))} \quad (6)$$

The input impedance for this section is then used as the load impedance for the transmission line segment at the top of the cell. The input impedance equation is then used again with these values to calculate the input impedance at that point in the transmission line model. This input impedance is then placed in parallel with the admittance from the shunt capacitance due to the change in the inner conductor diameter. This is then used in turn as the load impedance to calculate the input impedance to the small transmission line segment at the very top of the cell. This, finally, is placed in parallel with the admittance from the capacitance formed by the step discontinuity in the outer conductor's diameter at the top of the cell. The result of this calculation represents the frequency dependent input impedance for the entire cell. The reflection characteristics are simple to calculate at this point using the equation below.

$$\Gamma = \frac{Z_{in} - 50}{Z_{in} + 50} \quad \text{(Lonngren 2007)} \quad (7)$$

The calculations for the capacitances due to the conductor diameter discontinuities are not simple. Fortunately these discontinuities are located in the section

of the cell which is not intended to contain a sample, so while they are frequency dependent impedances, there is no concern of dramatic change in capacitance due to new dielectric media being introduced into the system. The susceptance of the shunt capacitors can be calculated via the system of equations shown in appendix A. (Marcuvitz 1986) However, an experiment was conducted in which the cell was fitted with a matched load termination During this experiment it was observed that the discontinuities produced very little reflection on their own.

3.3 Permittivity Calculation Algorithm

To estimate the permittivity of a measured sample, a numerical analysis was performed on the data. This was accomplished by calculating the Square Error (SE) between points in the measured data and points generated by the MatLab simulation. This calculation was performed on both the real and imaginary reflection coefficients for 201 frequencies evenly distributed from 50 to 400 MHz. The mean was taken of the 201 different SE calculations to provide the Mean Square Error (MSE). This process was repeated for 900 possible relative permittivity values ranging from 0.1 to 90.0. A minimization was then performed to estimate the relative permittivity of the sample. The procedure and the results it produced are discussed in greater detail in the Findings chapter which follows. Figure 3.4 below shows a flowchart detailing the algorithm's behavior.

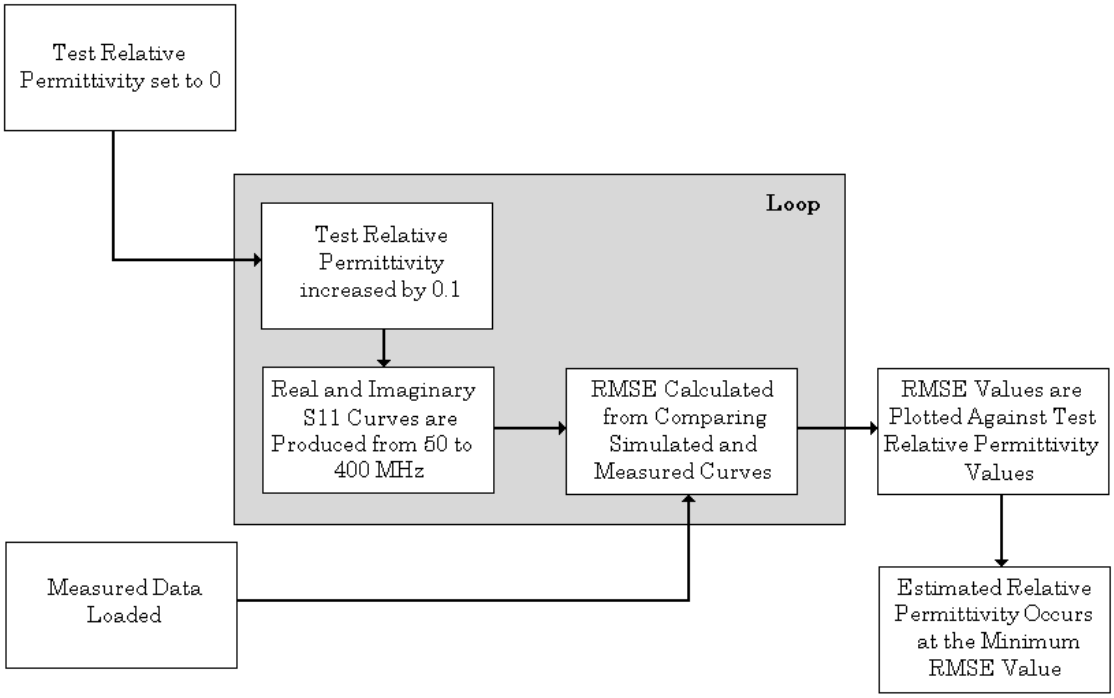

Figure 3.4. Algorithm Flowchart

3.4 Load Adjustments

Early simulations in the study showed a low degree of accuracy. While attempting to pinpoint the source of these inaccuracies it was found that the simulation was very sensitive to small changes in the termination load. In an effort to improve the simulation's performance, the termination load at the base of the sample chamber was adjusted for each sample material until the closest approximation could be found. This will be discussed in greater detail in chapter 4.

CHAPTER IV

FINDINGS

4.0 Load Issues

The simulation proved to be very sensitive to changes in the load at the end of the transmission line. Figure 4.1 below shows the changes in the simulation for Teflon as the load is varied.

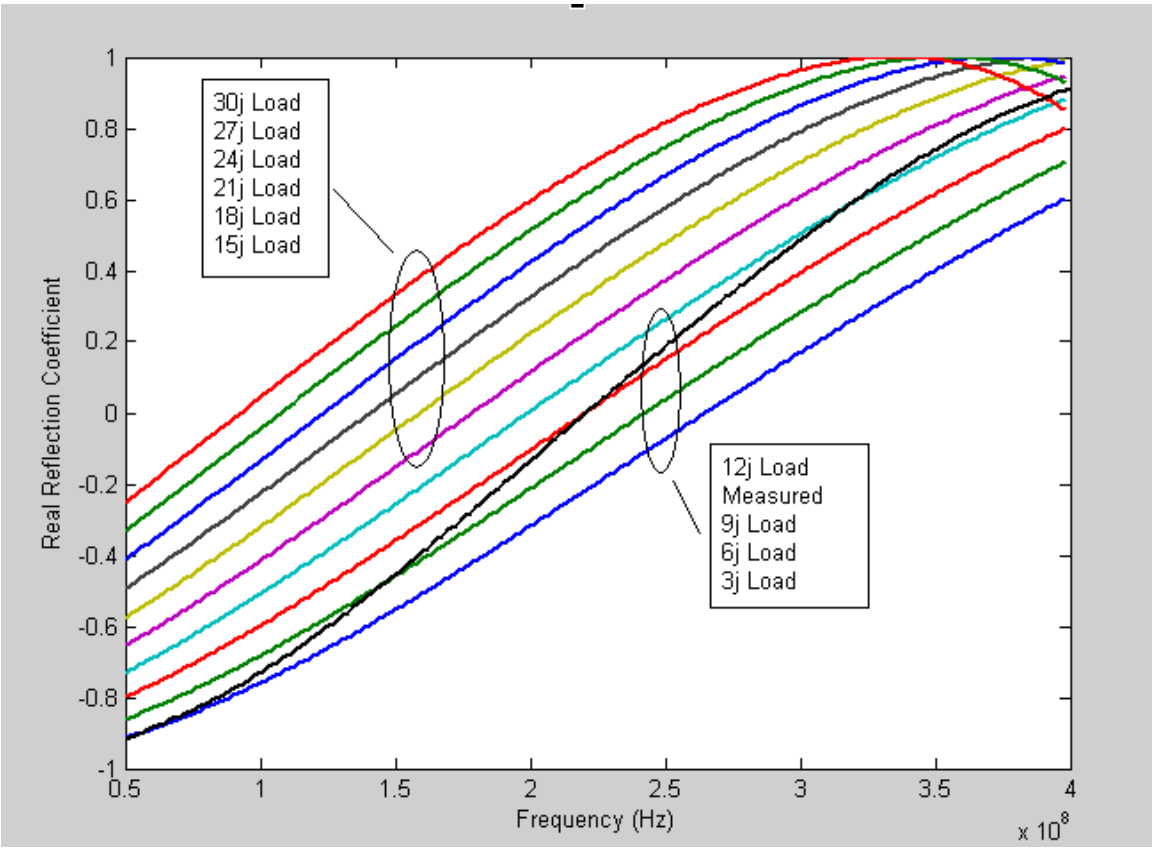

Figure 4.1. Teflon Simulation As Load Is Varied.

As seen in Figure 4.1, the reflection characteristics of the simulated system vary strongly as the load changes in small ways. This behavior indicates that the model is highly susceptible to error from inaccuracies in the load. Because the system is real, it is impossible to assume a perfect short circuit at the bottom of the cell. As such, some load will always be present. Figure 4.2 below shows the transmission line model with a load added at the end.

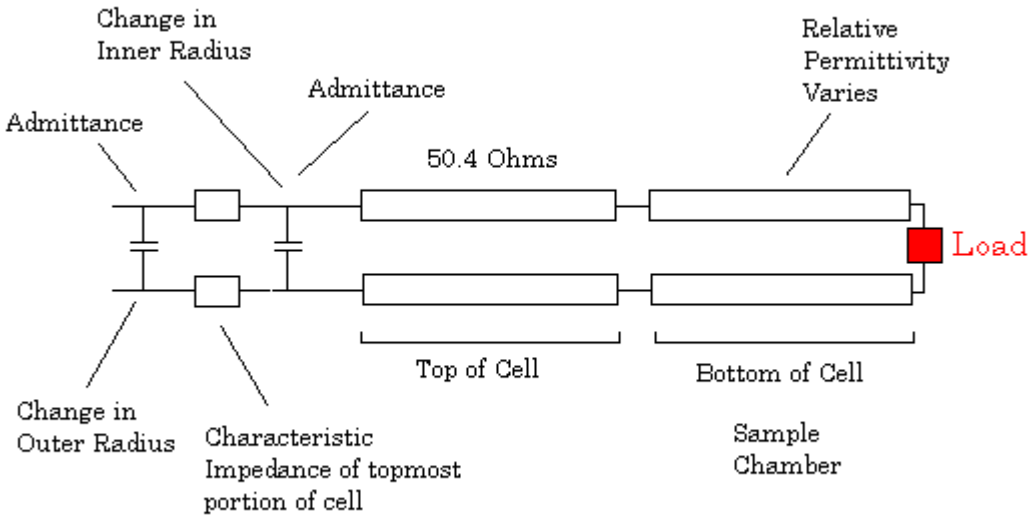

Figure 4.2. Transmission Line Model with Load

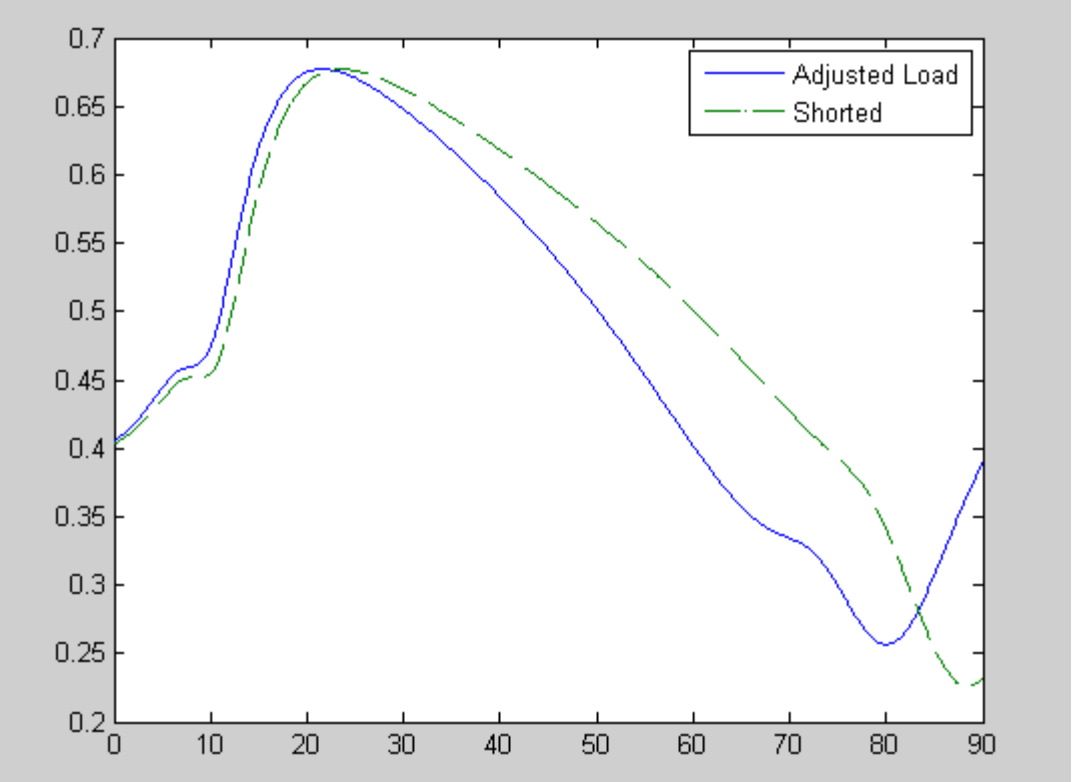

Figure 4.3. Load Comparison for Distilled Water

Figure 4.3 above shows the RMSE plots of distilled water for two different loads. The first of which is the adjusted load for distilled water, and the second is for the case of a short circuit termination. Note that for the idealized case of the short circuit termination the lowest error occurs much closer to 90 than 80. Table 2 below shows the load impedances used for each simulation.

Table 2. Load Impedances

Sample	Assumed Relative Permittivity	Load Impedance
Teflon	2.1	0.2+9j
Water	80.1	0.0+1j
Air	1.0	0.2+9j

Note that in the frequency range of operation, the load impedances in table 2 could be produced by an inductance as small as 6 nH. With this in mind it seems likely that this

experiment could be improved by altering the cell to have a specific known load in the bottom of the cell such that there is no longer a short, but is also not matched to the rest of the transmission line. A non-zero load would reduce the effect of noise in the load on the transmission line model significantly. However, it is important that no gap be left between the bottom plate of the cell and the center conductor. Leaving such a gap will cause a frequency dependence load in the form of a capacitance. The fringing effects will interact with the sample under test, complicating the system further. Sections 4.1, 4.2, and 4.3 investigate the algorithm's behavior when the adjusted loads shown in table 2 are used for the termination load in the transmission line equations. The algorithm appears in figure 3.4.

4.1 Teflon Analysis with Load Correction

A Teflon sample was cut to fit snugly within the sample chamber for this test, filling it completely. Figure 4.4 below shows a plot comparing the simulated data and measured data for the Teflon sample. The simulation operated under the premise that Teflon had a permittivity of approximately 2.1 at room temperature and a conductivity of 10E-24S/m. (Matweb 2010)

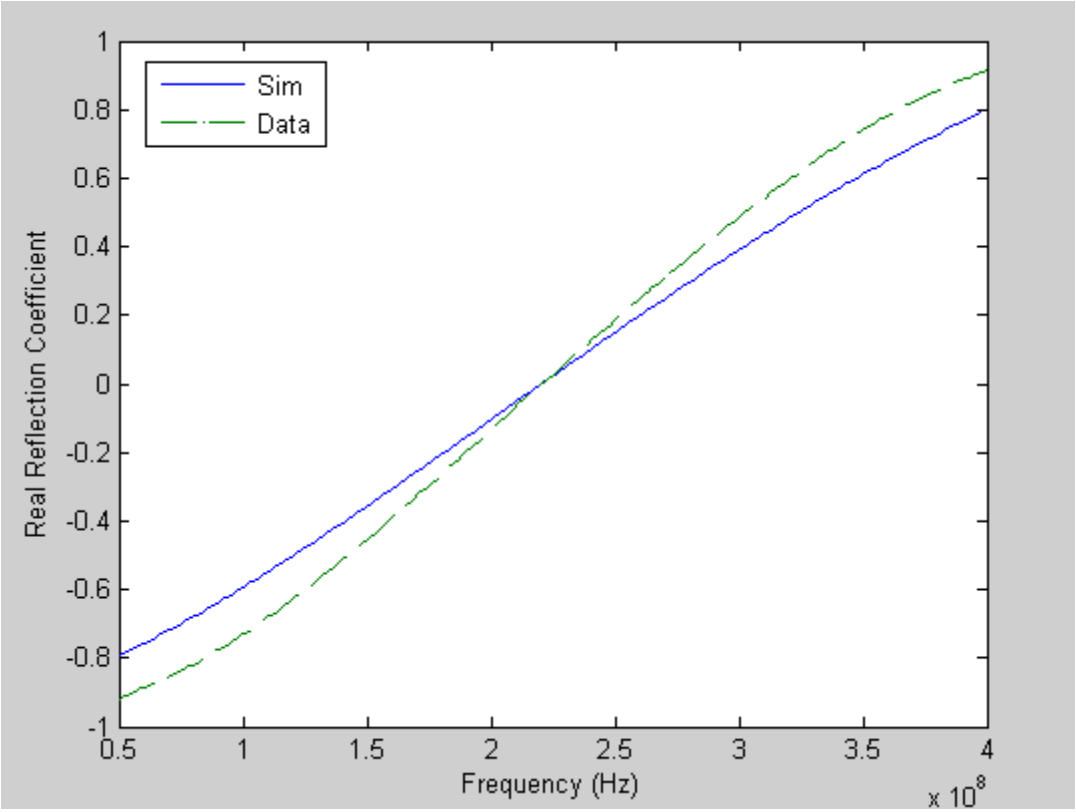

Figure 4.4. Comparison of Real Reflection Coefficient Data and Simulation for Teflon

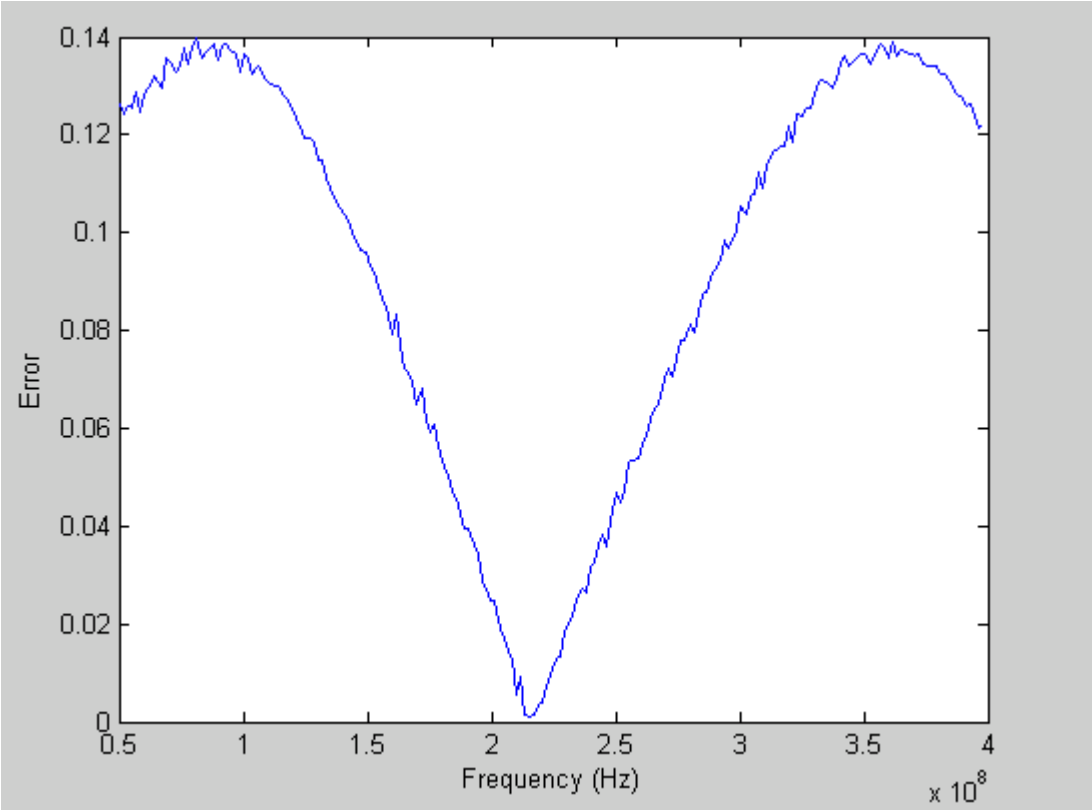

Figure 4.5. Magnitude of Error between Real Reflection Coefficient Data and Simulation

In order to arrive at an estimate of the relative permittivity, a minimization of a root mean square error (RMSE) calculation was implemented. This was done using the equation shown below. In this equation S is the array of simulation points, and D is the array of measured data points from the VNA. 201 points of data were collected and simulated. The points are represented by k.

$$RMSE = \left(\sum_{k=1}^{201} \frac{(S_k - D_k)^2}{201} \right)^{0.5} \quad \text{(Stark, 2002)} \qquad (8)$$

Figure 4.5 shows the magnitude of the error of each frequency point plotted in Figure 4.4. These points can be used to calculate a Root Mean Square Error (RMSE) for the measurements. For a relative permittivity of 2.1, an RMSE of 0.1036 was calculated.

Figure 4.6 shows the plot of the simulated imaginary reflection coefficient and the plot of the measured imaginary reflection coefficient. Again, Teflon was assumed to have a relative permittivity of approximately 2.1 and a conductivity of 10E-24 S/m (MatWeb 2010). The magnitude of error of the simulated versus measured data is shown in Figure 4.7. The RMSE for this data set was calculated to be 0.1098.

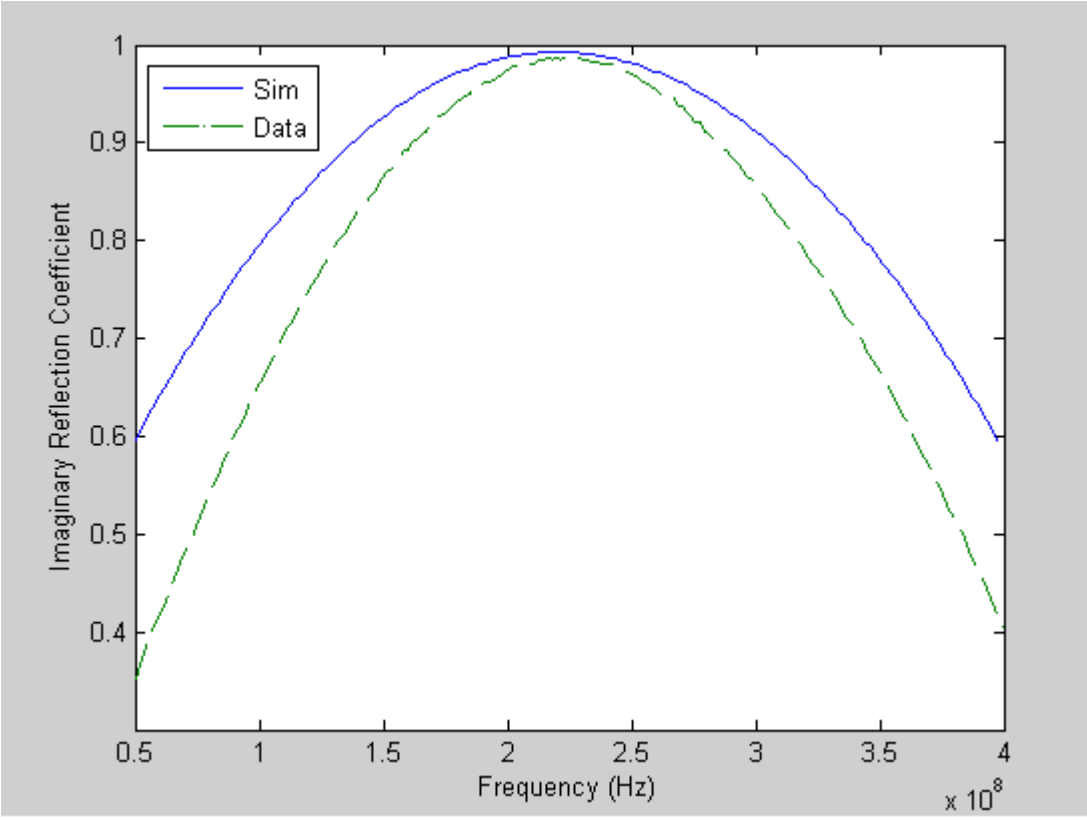

Figure 4.6. Comparison of Imaginary Reflection Coefficient Data and Simulation for Teflon

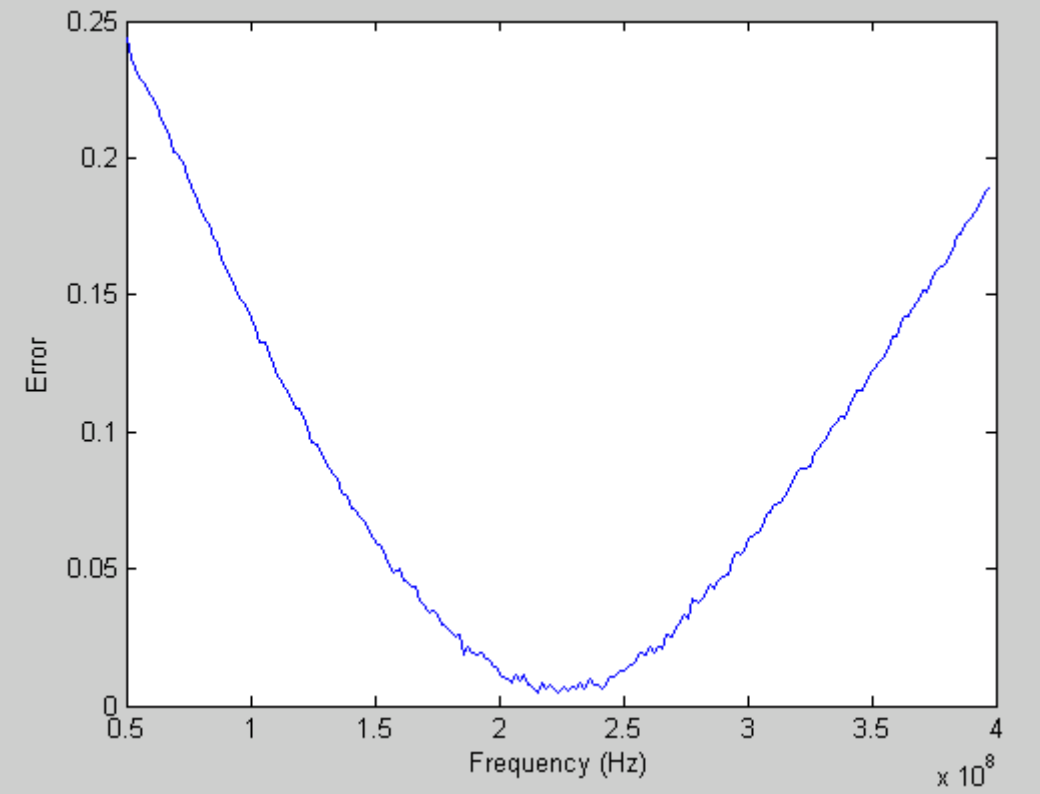

Figure 4.7. Magnitude of Imaginary Error

The plots in Figure 4.8 and Figure 4.9 show the RMSE calculated from equation 8 as the set of simulated points in S is recalculated for 900 possible relative permittivity matches ranging from 0.1 to 90.0. The top value of 90.0 was chosen to incorporate the full range of expected relative permittivity values while still allowing for error in the measurement of pure water samples. The simulation generates a real and imaginary reflection curve based on the relative permittivity value to be tested, and then determines the RMSE between each simulated curve and the respective curve generated by the VNA for the sample under test. Figure 4.8 and Figure 4.9 shows the RMSE calculation for each potential relative permittivity calculated by the simulation compared to the data gathered with the VNA using a Teflon core as the sample under test. The objective is a minimization, so the estimated relative permittivity is said to be the value which causes the lowest RMSE to be produced. However, observation of Figure 4.8 and Figure 4.9

both show a span of low RMSE around the estimated relative permittivity. Table 3 shows real reflection coefficient data on the RMSE at the known value of the permittivity of the Teflon core, as well as the data gathered at the calculated relative permittivity value arrived at by the previously described algorithm. Table 4 is the same data set presented for the imaginary component of the data.

Table 3. Real Reflection Coefficient Analysis of Teflon

Permittivity	Root Mean Square Error	Note
2.1	0.1036	Assumed Relative Permittivity of Teflon Sample
2.8	0.0834	Lowest RMS Error

Table 4. Imaginary Reflection Coefficient Analysis of Teflon

Permittivity	Root Mean Square Error	Note
2.1	0.1098	Assumed Relative Permittivity of Teflon Sample
2.9	0.0884	Lowest RMS Error

While there is a degree of error in the calculated permittivity in comparison to the known permittivity, the RMSE value for the known permittivity is close to that of the lowest calculated error. Inspection of Figure 4.8 and Figure 4.9 also show that the known relative permittivity does fall within the low error region in both data plots. As expected, relative permittivity values that are far from the known relative permittivity have a significantly higher error than the either the estimated or known relative permittivity. Additionally, disagreement in the permittivity is expected due to noise in the system, possible impurities in the sample, limitations in the accuracy of the measurement equipment, and most significantly the limitations of the mathematical model as described in the Load Issues section, section 4.1.

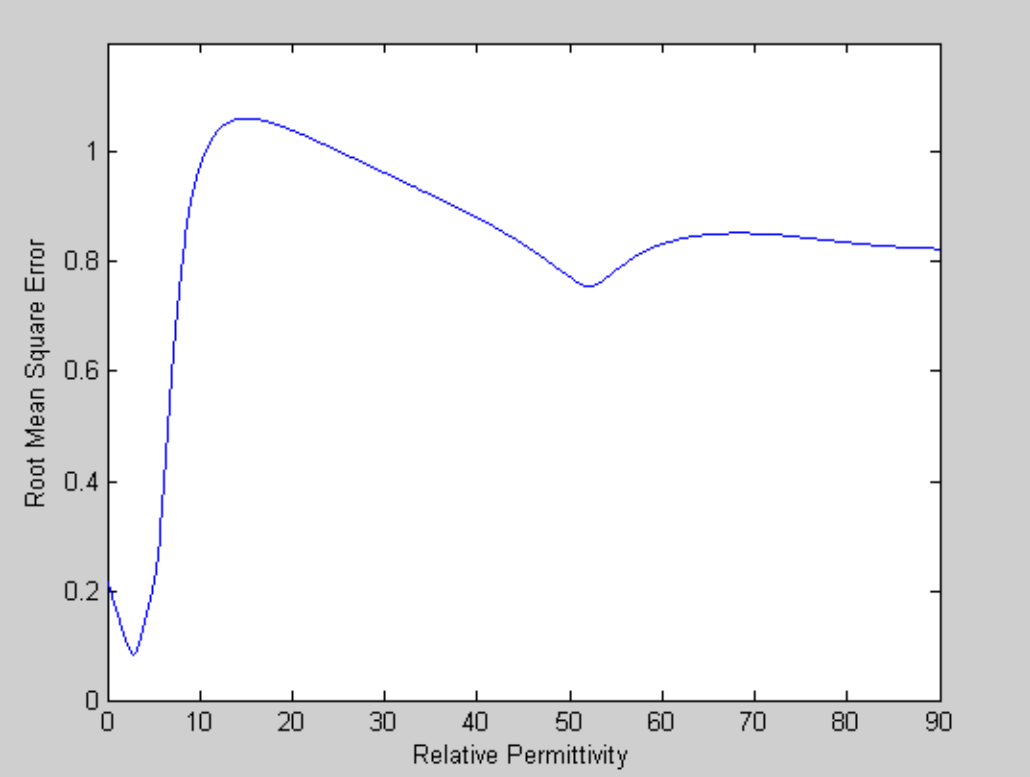

Figure 4.8. Real Root Mean Square Error for Test Relative Permittivity.

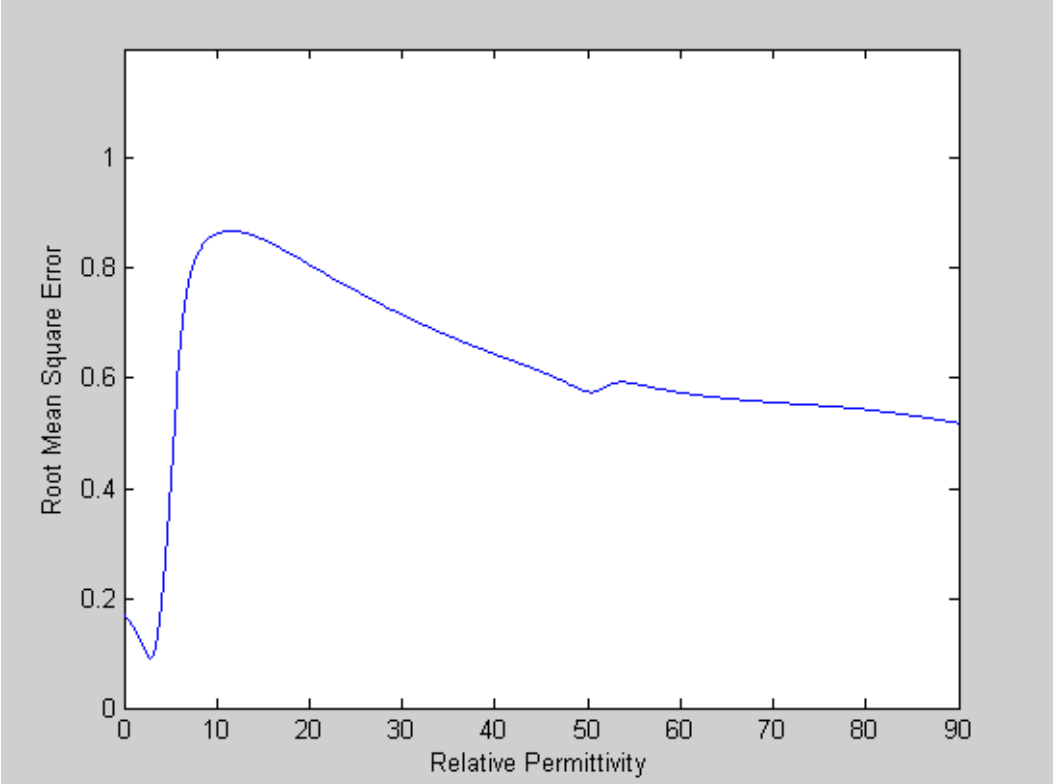

Figure 4.9. Imaginary Root Mean Square Error for Test Relative Permittivity

4.2 Distilled Water Analysis with Load Correction

The experiment was repeated with distilled water. Below, in figure 4.10, is a plot of the simulated data and measured data for distilled water. For the simulated data, a relative permittivity of 80.1 was used, and the conductivity was 0.5 S/m.

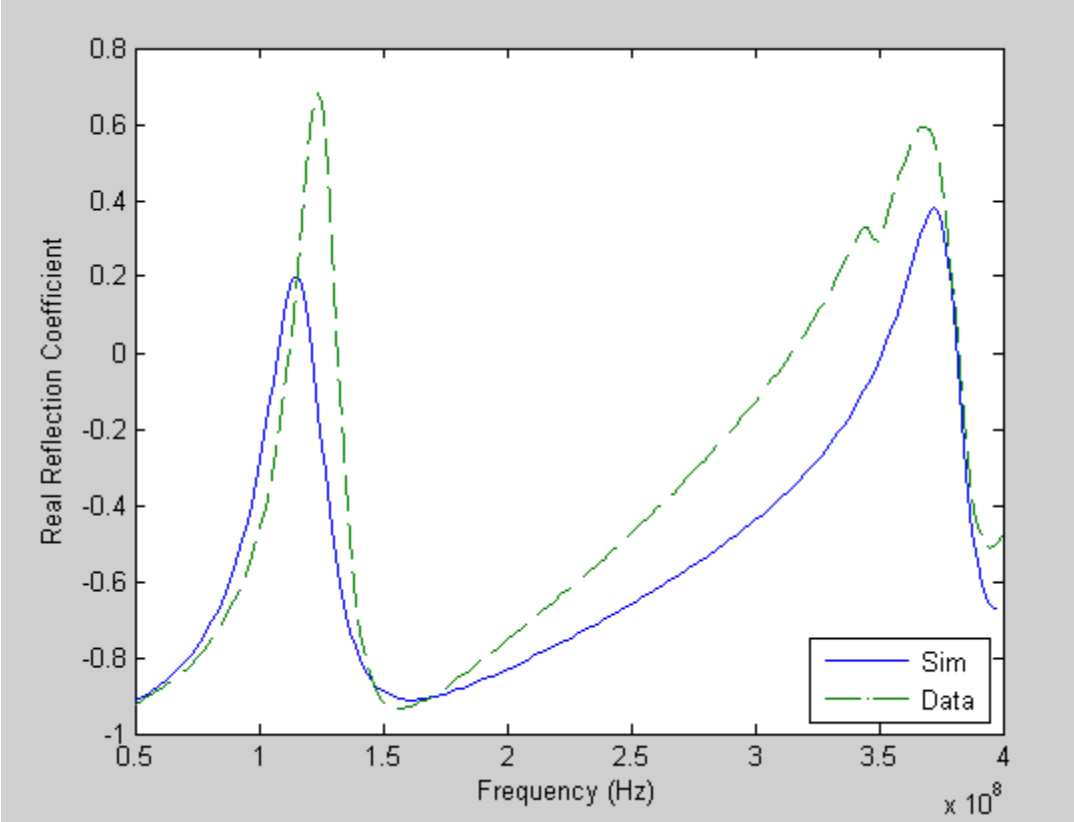

Figure 4.10. Distilled Water Real Reflection Coefficient Comparison

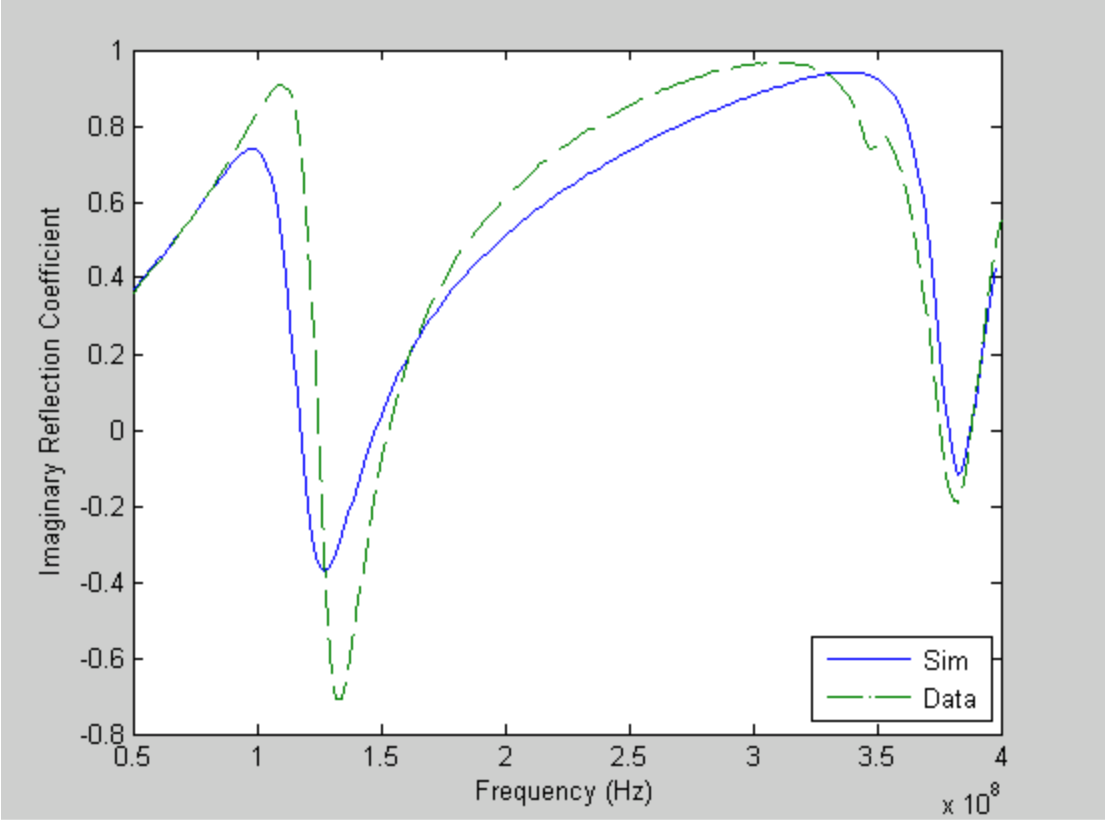

Figure 4.11. Distilled Water Imaginary Reflection Coefficient Comparison

Figure 4.11 above if the simulated and measured data for the imaginary reflection coefficient. Both Figure 4.11 and Figure 4.10 show a rough match between the simulated and measured data. An RMSE minimization was performed on the real and imaginary reflection coefficients for distilled water to determine which relative permittivity value was the closest match. The result from these evaluations is plotted below in Figure 4.12 and Figure 4.13.

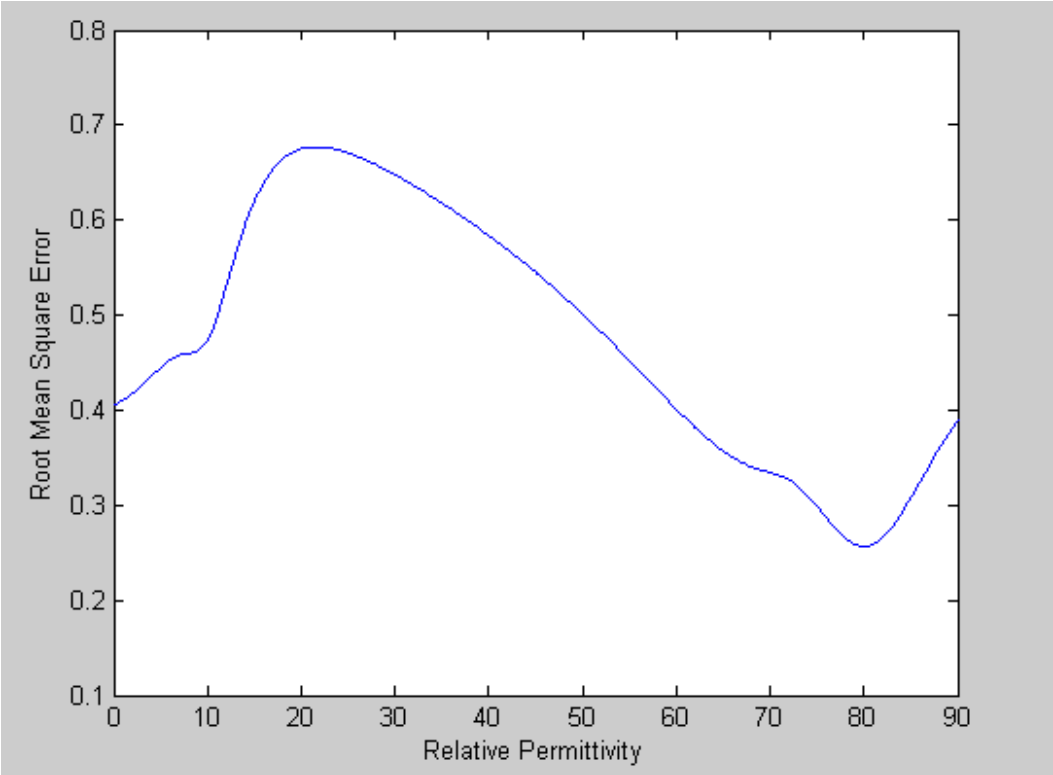

Figure 4.12. Real Reflection RMSE Versus Permittivity For Distilled Water

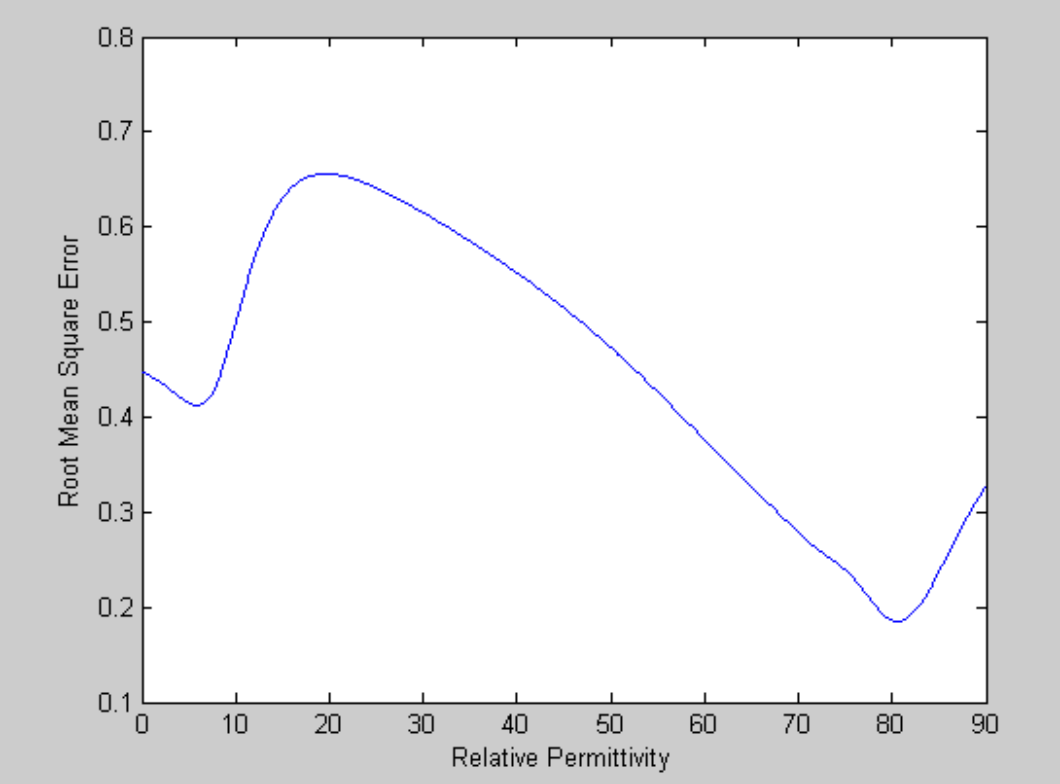

Figure 4.13. Imaginary Reflection RMSE Versus Permittivity For Distilled Water

Table 5. Distilled Water Real Reflection Coefficient Analysis

Permittivity	Root Mean Square Error	Note
80.1	0.2568	Assumed Relative Permittivity of Distilled Water
80.0	0.2568	Lowest RMS Error

Table 6. Distilled Water Imaginary Reflection Coefficient Analysis

Permittivity	Root Mean Square Error	Note
80.1	0.1858	Assumed Relative Permittivity of Distilled Water
80.6	0.1849	Lowest RMS Error

Table 5 and 6 show the results of the RMSE minimization. The relative permittivity estimation for distilled water produced an estimated permittivity closer to the assumed permittivity value than the estimation for Teflon. However, the best estimates for both distilled water tests did produce a larger calculated Root Mean Square Error than the tests for Teflon. Higher accuracy in the relative permittivity estimation is most likely due to the increased electrical length in the cell when the sample chamber is filled with distilled water.

4.3 Air Analysis with Load Correction

The experiment was repeated again with no sample in the sample chamber. For this case, the simulation assumed that the sample chamber was filled with air, and had an approximate conductivity of .55*10^-14 S/m. Figure 4.14 and Figure 4.15 show the comparison of the simulated data and the measured data for the real and imaginary reflection coefficient respectively. The simulation was run under the condition that air had a relative permittivity of 1.0.

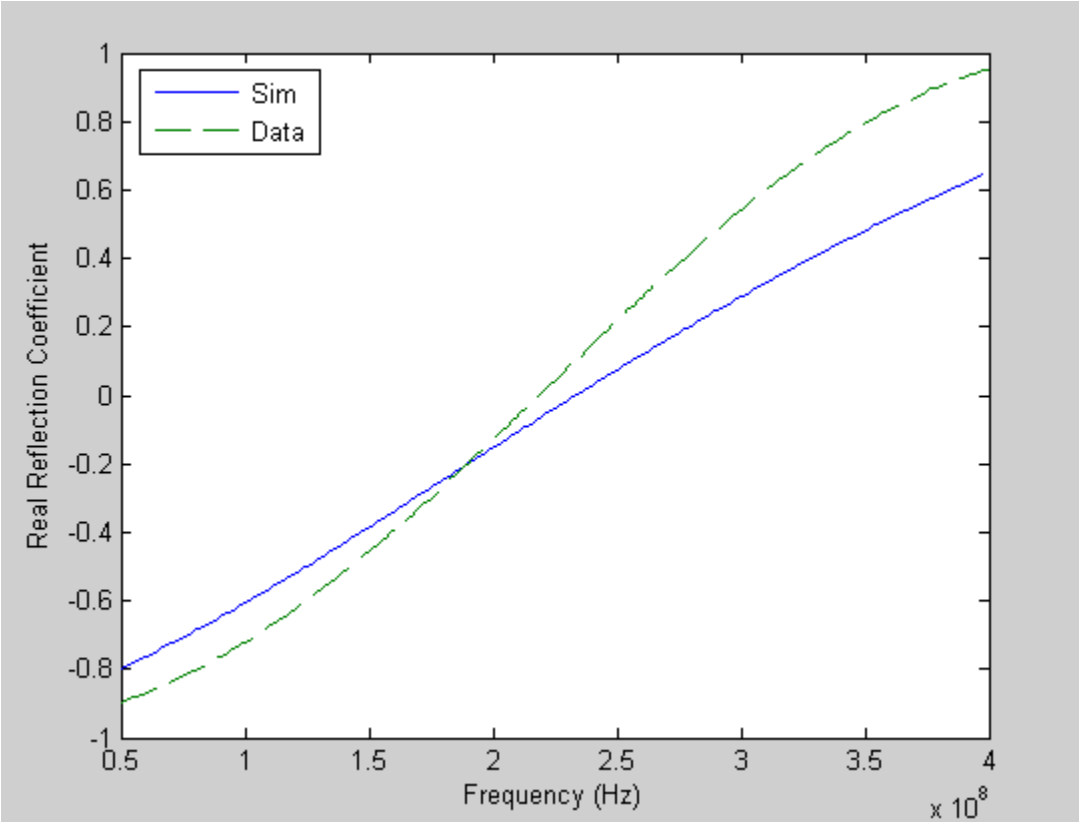

Figure 4.14. Real Reflection Coefficients of Air

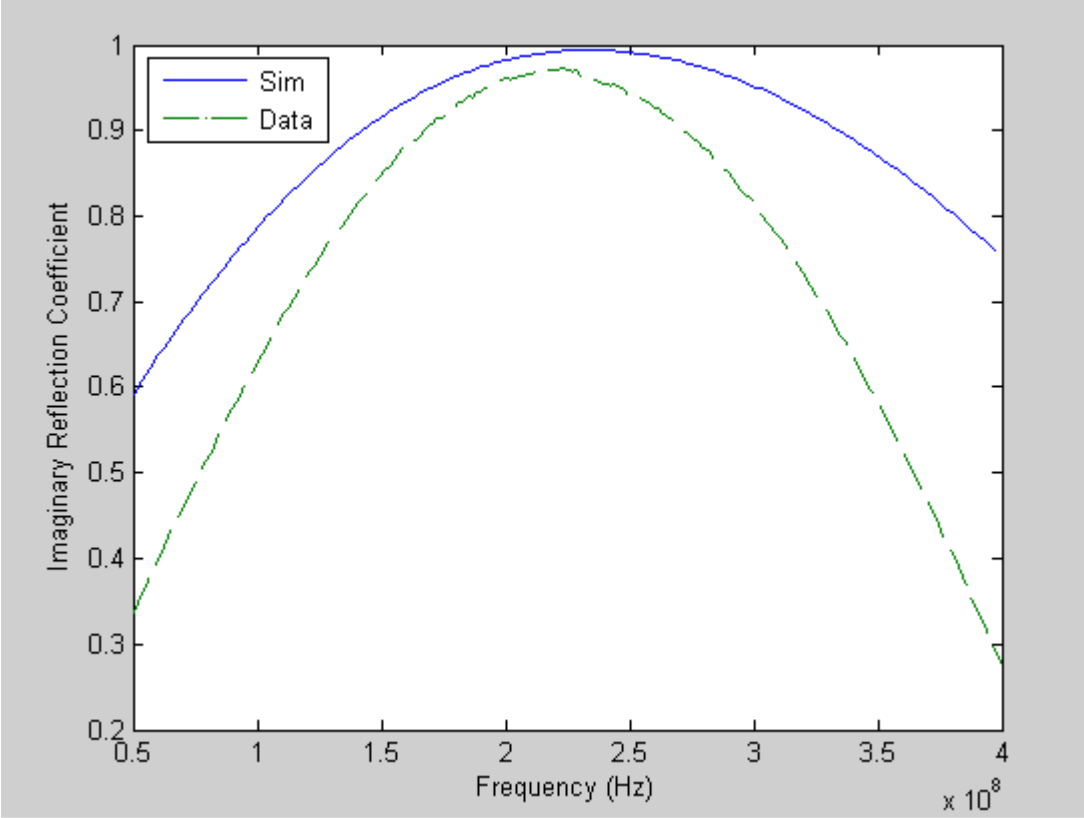

Figure 4.15. Imaginary Reflection Coefficients of Air

While neither the real or imaginary reflection coefficient simulation matches very closely to the measured data, both exhibit a similar structure over the frequency range. Figure 4.16 and Figure 4.17 follow. They show the RMSE plots for the reflection coefficients of the air samples versus simulation data in the same manner as in the previous experiments on Teflon and distilled water samples.

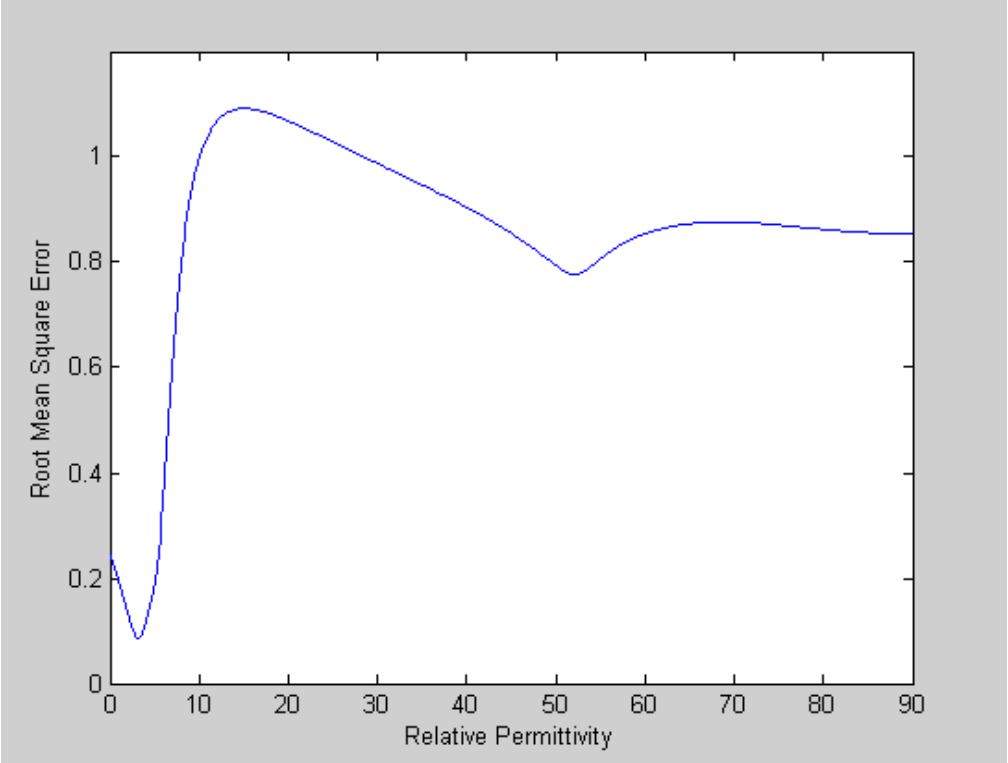

Figure 4.16. RMSE Analysis of Real Coefficients for Air Sample

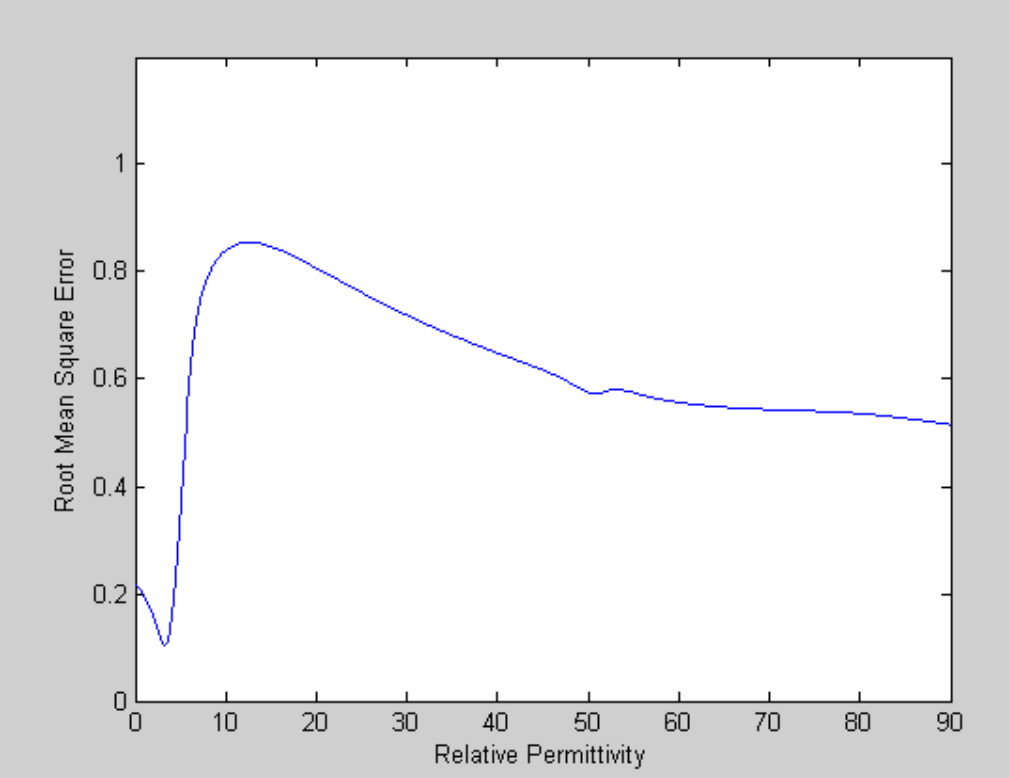

Figure 4.17. RMSE analysis of Imaginary Coefficients for Air Sample

It is interesting to note the similar appearance in the RMSE plots for the air data when compared to the Teflon data. Since both of these samples exhibit a very low conductivity and a low relative permittivity it is reasonable to expect these samples to produce very similar results. Below in table 7 and 8, the RMSE of the real and imaginary scans are shown for the assumed relative permittivity of 1, as well as the point where the simulation indicates a minimum error has occurred. While the lowest RMS error does not occur at the assumed relative permittivity, it is important to note that in both the real and imaginary comparison, the assumed relative permittivity lies within a region of low Root Mean Square Error.

Table 7. Air Sample Real Reflection Coefficient Analysis

Permittivity	Root Mean Square Error	Note
1.0	0.1949	Assumed Relative Permittivity of Air
3.2	0.0853	Lowest RMS Error

Table 8. Air Sample Imaginary Reflection Coefficient Analysis

Permittivity	Root Mean Square Error	Note
1.0	0.1955	Assumed Relative Permittivity of Air
3.3	0.1026	Lowest RMS Error

4.4 Comparison of Non-Adjusted to Adjusted Termination Loads

Repeating the same treatment of data described in section 4.1, 4.2, and 4.3 it quickly becomes clear that a short circuit load is undesirable. Table 9 contains the RMSE value found for the shorted load and adjusted load case when measured data is compared to simulated data at the assumed relative permittivity value for each of the three tested samples. Air samples were assumed to have a relative permittivity of 1.0. Teflon samples

were assumed to have a relative permittivity of 2.1. Distilled water samples were assumed to have a relative permittivity of 80.1.

Table 9. Comparison of RMSE Measurements for Shorted and Adjusted Loads

Sample	Shorted Load RMSE	Adjusted Load RMSE	Ratio
Air (Real)	0.3886	0.1949	50.15%
Air (Imaginary)	0.2333	0.1955	83.80%
Teflon (Real)	0.3271	0.1036	31.67%
Teflon (Imaginary)	0.1796	0.1098	61.14%
Distilled Water (Real)	0.3390	0.2568	75.75%
Distilled Water (Imaginary)	0.2800	0.1858	66.36%

Note that in all six cases the adjusted load produced a lower RMSE value at the assumed relative permittivity. In most cases this was significantly lower with Teflon's real reflection coefficient showing the most improvement.

Table 10. Comparison of Permittivity Estimates for Shorted and Adjusted Loads

Sample	Shorted Load Estimated Permittivity	Error	Adjusted Load Estimated Permittivity	Error
Air (Real)	8.7	770%	3.2	220%
Air (Imaginary)	7.1	610%	3.3	230%
Teflon (Real)	8.6	310%	2.8	33.3%
Teflon (Imaginary)	6.6	214%	2.9	38.1%
Distilled Water (Real)	88.4	10.36%	80.0	0.12%
Distilled Water (Imaginary)	88.9	10.99%	80.6	0.62%

Table 10 shows the algorithm's permittivity estimates for each sample as estimated from the real and imaginary reflection characteristics. Estimates for the shorted load case and the adjusted load case are provided. Inspection of table 10 reveals that the adjusted loads consistently produce a smaller error in the permittivity estimate. In some cases the error is reduced by several orders of magnitude.

4.5 Usefulness of RMSE Analysis

RMSE is beneficial for this analysis as the mathematical simulation and transmission line model of the cell are limited in their accuracy, and as such it is unlikely that a perfect match between simulated and measured data would ever be found. RMSE analysis finds the closest overall match. This is desirable because no one frequency point is more significant in the measurement than any other. RMSE diminishes errors due to random variables such as noise as it allows for analysis of a large number of data points to find the best overall fit for the entire data set as opposed to attempting to simply match the simulated and measured coefficient for a specific frequency or matching locations of peaks.

CHAPTER V

CONCLUSION

The goals of this thesis were as follows:

1. Identify the strengths and weaknesses in the previous transmission line model of the coaxial cell.

2. Select and mathematically describe an alternative model to address known weaknesses in the previous model.

3. Produce a simulation tool for the model.

4. Discuss strengths and weaknesses of the new model.

5.1 Accomplishments

The original transmission line model was shown to be lacking elements to account for the abrupt changes in the radius of both the inner, and outer conductor of the coaxial cell. The model was also found to not account for the topmost portion of the coaxial cell. The model was improved upon via incorporating two susceptances into the model to account for the two discontinuities. A transmission line segment was also added between these two susceptances to account for the short segment of the cell which was previously ignored. Due to the problems associated with a short circuit termination, it is difficult to assess the magnitude of the benefit of incorporating these missing features. However, it is more technically correct to include them.

The thesis also suggested significant weaknesses in the previous design of the coaxial cell. A flaw was found in that the gap between the bottom plate of the cell and the center conductor causes a capacitance that varies its traits with frequency and the permittivity of the sample under test. An attempt was made to address this undesirable aspect by shorting the center conductor to the bottom plate. A series of Matlab scripts were produced to simulate the behavior of the modified cell. The scripts are capable of comparing simulated data to measured data and calculating the discrepancy between the two, as well as estimate the permittivity of the sample under test.

Shorting the center conductor to the bottom plate removed the capacitance from the model, study showed that attempting a near 0 ohm termination load caused behaviors in the simulation that were unpredictable due to the small size of the termination load and the significance of its impact on the simulated reflection characteristics. Analysis showed that better knowledge of the true termination load could cause dramatically improved estimations of the relative permittivity.

5.2 Future Work

To better expand the research, a new coaxial cell should be built. The new cell should have two major adjustments. First, the center conductor in the top section of the shell should be altered such that the radius of the inner conductor gradually increases in radius rather than changing abruptly. This tapered top section has been used in other designs. (Huang 2000). Second, a load should be added to the bottom of the inner conductor between the conductor and the bottom lid. This load should be a disk of the same radius as the center conductor and should fit snugly between the center conductor and the bottom lid. This load should not match the characteristic impedance of the cell.

Currently it is essential to know the conductivity of the sample under test. A lack of knowledge of the conductivity of the sample prevents measurement. However, the objective is to assess the volumetric soil moisture which limits the traits of the possible sample under test to soil and water. It seems reasonable to assume that the relative permittivity estimation could be improved by incorporating an analysis of the sample's conductivity.

Finally, the work can be expanded by developing an equation to convert the relative permittivity measurements to an estimation of the volumetric water content ratio. This equation would then need to be tested against real soil samples using the methods described in this document. Additionally, a repeat of the original experiment should be performed using the new model. This would require gathering a number of soil samples, estimating the relative permittivity, and comparing it to measured soil moisture values. It

may also be prudent to investigate alternative simulation methods to model the coaxial cell.

REFERENCES

Gelalecha, A. 2000. Reconstruction Algorithm for Predicting Profiles of Permittivity and Conductivity from Surface Reflection Measurement. Unpublished MS Thesis. Stilwater, OK: Oklahoma State University, Department of Electrical and Computer Engineering.

Arnold, J. A. 1990. The Development Of A Dielectric Based Soil Moisture Sensor. Unpublished MS thesis. Stillwater, OK: Oklahoma State University, Department of Biosystems and Agricultural Engineering.

Donahue, R.L., Miller, R. W., and Shickluna, J. C. 1977. *Soils An Introduction to Soils and Plant Growth.* Englewood Cliffs, NJ: Prentice Hall.

Duvall, J. D. 2010. Electromagnetic Analysis of Soil Moisture via Reflection Characteristics*.* 2010 ASABE Annual International Meeting

Hanks, R. J. and Ashcroft, G. L. 1980. *Applied Soil Physics*. Berlin Heidelberg Germany: Springer-Verlag

Huany, Y. 2000. Design, calibration, and data interpretation for a one-port large coaxial dielectric measurement cell. Institute of Physics Publishing.

Jorgensen, J.L., Edison, A.R., Nelson, S.O., Stetson, L.E. 1970. A Bridge Method for Dielectric Measurements of Grain and Seed in the 50 to 250 MHz Range. In *Transaction of the ASAE,* 13(1):18-20,24.

K. H. Lee, N. Zhang, W. B. Kuhn, G. J. Kluitenberg. 2007. A Frequency-Response Permittivity Sensor for Simultaneous Measurement of Multiple Soil Properties: Part I. The Frequency-Response Method.2007. A Frequency-Response Permittivity Sensor for Simultaneous Measurement of Multiple Soil Properties: Part I. The Frequency-Response Method. ASABE

Logsdon, S. D. 2005. Soil Dielectric Spectra from Vector Network Analyzer Data. Soil Sci. Soc. Am. J.

Lonngren, K.E., Savov, S.V., and Jost, R. J. 2007. *Fundamentals of Electromagnetics with MATLAB.* Raleigh, NC: Scitech Publishing, Inc.

Marcuvitz, M. 1986. *Waveguide Handbook.* London, UK: Peter Peregrinus Ltd.

MatWeb. 2009. Overview of Materials for PTFE, Extruded. Blacksburg, VA.: Automation Creations, Inc. Available at: www.matweb.com. Accessed 8 May 2010.

Nelson, S. O. Dielectric Properties of Agricultural Products Measurements and Applications. In *IEEE Transactions on Electrical Insulation* 1991 vol 26 IEEE

Nelson, S. O. Dielectric Spectroscopy in Agriculture. In *Journal of Non-Crystalline Solids* 2005 vol 351 International Conference on Broadband Dielectric Spectroscopy

Rial, W.S., Han, Y.J. Assessing Soil Water Content Using Complex Permittivity. In *Transactions of the ASAE*, 1979-1985 vol 43 American Society of Agricultural Engineers.

Stark, H. and Woods, J. W. 2002. *Probability and Random Processes.* Upper Saddle River, NJ: Prentice Hall.

Topp, G. C., J. L. Davis, and A. P. Annan. 1980. Electromagnetic determination of soil water content: measurements in coaxial transmission lines. Water Resour. Res. 16: 574-582

Trabelsi, Samir, 2010. Microwave Moisture Meter for Rapid and Nondestructive Grading of Peanuts. ASABE International Meeting.

APPENDICES

Appendix A Shunt Capacitance Calculation

Equations 9 through 20 below can be used to calculate the susceptance Y_o which occurs in the transmission line model when the radius of the inner conductor undergoes an abrupt, discontinuous change. The susceptance for the change in the radius of the outer conductor can be calculated similarly. This method is outlined more thoroughly in Marcuvitz, 1986.

Nomenclature List

a = inner conductor radius before discontinuity
b = inner conductor radius after discontinuity
c = outer conductor radius
γ_1 =complex propagation constant

$$\frac{B}{Y_o} = \frac{2b_o A_1}{\lambda}\left[\begin{array}{l} 2\ln\left(\frac{1-\alpha^2}{4\alpha}\right)\left(\frac{1+\alpha}{1-\alpha}\right)^{\frac{1}{2}\left(\alpha+\frac{1}{\alpha}\right)} + 4\frac{A+A'+2C}{AA'-C^2} \\ +\frac{1}{2}\left(\frac{b_o}{\lambda}\right)^2\left(\frac{1-\alpha}{1+\alpha}\right)^{4\alpha}\left(\frac{5\alpha^2-1}{1-\alpha^2}+\frac{4}{3}\frac{\alpha^2 C}{A}\right)^2 + \frac{A_2}{2} \end{array}\right] \tag{9}$$

$$\alpha = 1-\delta = \frac{c-b}{c-a} \tag{10}$$

$$b_o = c-a \tag{11}$$

$$b_o' = c-b \tag{12}$$

$$A=\left(\frac{1+\alpha}{1-\alpha}\right)^{2\alpha}\frac{1+\sqrt{1-\left(\frac{b_o}{\lambda/2}\right)^2}}{1-\sqrt{1-\left(\frac{b_o}{\lambda/2}\right)^2}}-\frac{1+3\alpha^2}{1-\alpha^2} \tag{13}$$

$$A'=\left(\frac{1+\alpha}{1-\alpha}\right)^{2/\alpha}\frac{1+\sqrt{1-\left(\frac{b_o'}{\lambda/2}\right)^2}}{1-\sqrt{1-\left(\frac{b_o'}{\lambda/2}\right)^2}}-\frac{3+\alpha^2}{1-\alpha^2} \tag{14}$$

$$C=\left(\frac{4\alpha}{1-\alpha^2}\right)^2 \tag{15}$$

$$A_1=\frac{b}{a}\frac{\ln\left(\frac{c}{a}\right)}{\frac{c}{a}-1}\left(\frac{\frac{c}{b}-1}{\ln\left(\frac{c}{b}\right)}\right)^2 \tag{16}$$

$$A_2=\frac{\pi^2\frac{a}{b}}{\gamma_1\sqrt{1-\left(\frac{2b_o}{\gamma_1\lambda}\right)^2}}\frac{\frac{c}{a}-1}{\frac{J_o^2(\chi)}{J_o^2\left(\chi c/a\right)}-1}\left[\frac{J_o(\chi)N_o\left(\frac{\chi b}{a}\right)-N_o(\chi)J_o\left(\frac{\chi b}{a}\right)}{\frac{c}{b}-1}\right]^2$$
$$-\frac{1}{\sqrt{1-\left(\frac{2b_o}{\lambda}\right)^2}}\left(\frac{2}{\pi}\frac{b_o}{d}\sin\left(\frac{\pi d}{b_o}\right)\right)^2 \tag{17}$$

$$\chi=\frac{\pi\gamma_1}{c/a-1}=\chi_{01} \tag{18}$$

χ_{01} is the first non-vanishing root of:

$$J_o(\chi)N_o\left(\frac{\chi c}{a}\right) - N_o(\chi)J_o\left(\frac{\chi c}{a}\right) = 0 \tag{19}$$

This system of equations is constrained in that it is only valid provided that the applied field is rotationally symmetrical. Additionally, the wavelength of the field and the dimensions of the cell must meet the following requirement:

$$\lambda > \frac{2(c-a)}{\gamma_1} \tag{20}$$

These restrictions hold valid for both discontinuities. According to the dimensions of the cell, this equation system holds valid for all frequencies less than 5.5 GHz which contains the entire operating range of interest. (Marcuvitz, 1986)

Appendix B Matlab Programs

```
%Cell Analysis Program
%Simulation modified to allow for a relative permittivity to be
placed in
%the system.
%December 7, 2009.


%To use this program, frequency and reflection coefficient data must
be
%available in the workspace.
%VFreqData is a variable which is a 1 by 201 double, and contains
the
%frequencies in hertz.
%VRealData is a 1 by 201 double containing real reflection
coefficients.
%VImagData is a 1 by 201 double containing imaginary relfection
%coefficients



freq=50000000:1741294:400000000;

Z_c=50;
c=3*10^8;

lambda=c./freq;
Beta=2*pi./lambda;
mu=4*pi*10^-7;
omega=2*pi.*freq;




%diameters in mm. Used as a ratio only.
b=54.0;
a=23.647;
nail=3.15;

%properties of inserted dielectric media
o_air=.55*10^-14;   %conductivity for air
o_hexane=100*10^-12;   %conductivity for hexane
o_teflon=10^-24; %conductivity for teflon
o_water=.05;

o_bottom=o_water;


epsilon=8.854*10^-12;

Eps_Teflon=2.1;
Eps_water=80.1; %taken from wikipedia for 20* Celcius (80.1)
```

```
Eps_r=0;

for i=1:900

    Eps_r=i/10;
    Eps_test(i)=i/10;
cmedia=c/1.4;
lambdamedia=cmedia./freq;


%units in meters.
l_cellshortsection=.0083058;
l_celltop=.0568452;
l_cellbottom=.0637032;



Cap=4.9736*10^-10; %approximation trying to get data to fit a peak
at 160 MHz
gamma_bottom=(1i*mu*o_bottom.*omega-mu*Eps_r*epsilon.*omega.*omega);
gamma_bottom=sqrt(gamma_bottom);

gamma_top=(1i*mu*o_air.*omega-mu*1*epsilon.*omega.*omega);
gamma_top=sqrt(gamma_top);

%sample impedance value for capacitance from discontinuity. Value is
%calculated for 75 MHz.
ZCap=(-1i*.002653)^-1;



%Calculate complex propogation constant within coaxial cell.
Zo_CellTinyTop=(1i.*omega*mu)./(2*pi.*gamma_top)*log(b/nail);
%Characteristic Impedence of Cell VERY Top section
Zo_CellBottom=(1i.*omega*mu)./(2*pi.*gamma_bottom)*log(b/a);
%Characteristic Impedence of Cell Bottom section
Zo_CellTop=(1i.*omega*mu)./(2*pi.*gamma_top)*log(b/a);
%Characteristic Impedence of Cell Top section
%Z_Cap=1./(omega*1i*Cap);                        %Impedence of
capacitance.
%Z_Cap=0-1.8j;
%Z_Cap=0.2+9j; %for teflon
%Z_Cap=0+1j; %for water
%Z_Cap=0.2+9j; %for air.
Z_Cap=0+1j;



ZCellBottom=Zo_CellBottom.*(Z_Cap+Zo_CellBottom.*tanh(gamma_bottom.*
l_cellbottom))./(Zo_CellBottom+tanh(gamma_bottom.*l_cellbottom).*Z_C
ap); %Input impedence looking into bottom of cell.
```

```
ZCellTop=Zo_CellTop.*(ZCellBottom+Zo_CellTop.*tanh(gamma_top.*l_cell
top))./(Zo_CellTop+tanh(gamma_top.*l_celltop).*ZCellBottom); %Input
impedence looking into top of cell.

ZAdjunct=(ZCellTop.^-1+ZCap.^-1).^-1; %impedance of discontinuity
capacitance in parallel with the rest of the system.

ZCellTinyTop=Zo_CellTinyTop.*(ZAdjunct+Zo_CellTinyTop.*tanh(gamma_to
p.*l_cellshortsection))./(Zo_CellTinyTop+tanh(gamma_top.*l_cellshort
section).*ZAdjunct); %Input impedence looking into VERY top of cell.

%ZAdjunct=(ZCellTop.^-1+ZCap.^-1).^-1;
%Zin=Z_c*(ZAdjunct+Z_c.*tanh(gamma.*l_cable))./(Z_c+tanh(gamma.*l_ca
ble).*ZAdjunct);           %Input impedence looking into system.


%Now, account for capacitance from discontinuity in inner conductor
radius.

%ZAdjusted=ZAdjunct;
ZAdjusted=ZCellTinyTop;


GCoeff=(ZAdjusted-50)./(ZAdjusted+50);

%Calculate the RMSE from the reflection coefficiences.
RealError=((real(GCoeff)-VRealData).^2);
ImagError=((imag(GCoeff)-VImagData).^2);


TotalRealError(i)=(sum(RealError)/201)^.5;
TotalImagError(i)=(sum(ImagError)/201)^.5;
end

%print the real figure
figure;
plot(Eps_test,TotalRealError);
xlabel('Relative Permittivity');
ylabel('Root Mean Square Error');

%print the imaginary figure
figure;
plot(Eps_test,TotalImagError);
xlabel('Relative Permittivity');
ylabel('Root Mean Square Error');
```

```
%Cell Error Plotter Program
%Simulation modified to allow for a relative permittivity to be
placed in
%the system.
%December 7, 2009.

%To use this program, frequency and reflection coefficient data must
be
%available in the workspace.
%VFreqData is a variable which is a 1 by 201 double, and contains
the
%frequencies in hertz.
%VRealData is a 1 by 201 double containing real reflection
coefficients.
%VImagData is a 1 by 201 double containing imaginary relfection
%coefficients

freq=50000000:1741294:400000000;

Z_c=50;
c=3*10^8;

lambda=c./freq;
Beta=2*pi./lambda;
mu=4*pi*10^-7;
omega=2*pi.*freq;



%l_cell=.1273./lambda;

%diameters in mm. Used as a ratio only.
b=54.0;
a=23.647;
nail=3.15;

%properties of inserted dielectric media
o_air=.55*10^-14;   %conductivity for air
o_hexane=100*10^-12;   %conductivity for hexane
o_teflon=10^-24;%conductivity for teflon
o_water=.05;

o_bottom=o_water; %Set conductivity here.


epsilon=8.854*10^-12;

Eps_Teflon=2.1;
Eps_water=80.1; %taken from wikipedia for 20* Celcius (80.1)

Eps_r=80.1; %set relative permittivity to test here.
```

```
    Eps_test=Eps_r;
cmedia=c/1.4;
lambdamedia=cmedia./freq;



%units in meters.
l_cellshortsection=.0083058;
l_celltop=.0568452;
l_cellbottom=.0637032;



gamma_bottom=(1i*mu*o_bottom.*omega-mu*Eps_r*epsilon.*omega.*omega);
gamma_bottom=sqrt(gamma_bottom);

gamma_top=(1i*mu*o_air.*omega-mu*1*epsilon.*omega.*omega);
gamma_top=sqrt(gamma_top);

%sample impedance value for capacitance from discontinuity. Value is
%calculated for 75 MHz.
ZCap=(-1i*.002653)^-1;



%Calculate complex propogation constant within coaxial cell.
Zo_CellTinyTop=(1i.*omega*mu)./(2*pi.*gamma_top)*log(b/nail);
%Characteristic Impedence of Cell VERY Top section
Zo_CellBottom=(1i.*omega*mu)./(2*pi.*gamma_bottom)*log(b/a);
%Characteristic Impedence of Cell Bottom section
Zo_CellTop=(1i.*omega*mu)./(2*pi.*gamma_top)*log(b/a);
%Characteristic Impedence of Cell Top section
%Z_Cap=1./(omega*1i*Cap);                        %Impedence of
capacitance.
%This was removed.

%Z_Cap=0.2+9j; %for teflon
%Z_Cap=0+1j; %for water
%Z_Cap=0.2+9j; %for air
Z_Cap=0+1j;



ZCellBottom=Zo_CellBottom.*(Z_Cap+Zo_CellBottom.*tanh(gamma_bottom.*
l_cellbottom))./(Zo_CellBottom+tanh(gamma_bottom.*l_cellbottom).*Z_C
ap); %Input impedence looking into bottom of cell.
ZCellTop=Zo_CellTop.*(ZCellBottom+Zo_CellTop.*tanh(gamma_top.*l_cell
top))./(Zo_CellTop+tanh(gamma_top.*l_celltop).*ZCellBottom); %Input
impedence looking into top of cell.

ZAdjunct=(ZCellTop.^-1+ZCap.^-1).^-1; %impedance of discontinuity
capacitance in parallel with the rest of the system.
```

```
ZCellTinyTop=Zo_CellTinyTop.*(ZAdjunct+Zo_CellTinyTop.*tanh(gamma_to
p.*l_cellshortsection))./(Zo_CellTinyTop+tanh(gamma_top.*l_cellshort
section).*ZAdjunct); %Input impedence looking into VERY top of cell.




%ZAdjusted=ZAdjunct;
ZAdjusted=ZCellTinyTop;


GCoeff=(ZAdjusted-50)./(ZAdjusted+50);


%Calculates absolute value of error between simulation and gathered
data.
RealError=(abs(real(GCoeff)-VRealData));
ImagError=(abs(imag(GCoeff)-VImagData));




%plot figures
figure;
plot(freq,RealError);
xlabel('Frequency (Hz)');
ylabel('Error');

figure;
plot(freq,ImagError);
xlabel('Frequency (Hz)');
ylabel('Error');

figure;
plot(freq, real(GCoeff), VFreqData, VRealData);
xlabel('Frequency (Hz)');
ylabel('Real Reflection Coefficient');

figure;
plot(freq, imag(GCoeff), VFreqData, VImagData);
xlabel('Frequency (Hz)');
ylabel('Imaginary Reflection Coefficient');
```

```
%Root Finder Program
%use to see where Xi crosses a zero point.
a=.122;
c=2.127;

Xi=0:.002:2;

Value=BESSELJ(0,Xi).*BESSELY(0,Xi*c/a)-
BESSELY(0,Xi).*BESSELJ(0,Xi*c/a);
plot(Xi,Value);
```

```
%Discontinuity Program
%This program calculates the B over Y value described on page 310 of
The
%Waveguide Handbook.

a=.00155; %1.55mm
b=.012306; %12.306mm
c=.027013; %27.013mm
x=0:.025:1;
lambda = 4; %m

%x=0:.05:1;
%a=.10;
%b=[5.0,4.9,4.8,4.7,4.6,4.5,4.4,4.3,4.2,4.1,4.0,3.9,3.8,3.7,3.6,3.5,
3.4,3.3,3.2,3.1,3.0,2.9,2.8,2.7,2.6,2.5,2.4,2.3,2.2,2.1,2.0,1.9,1.8,
1.7,1.6,1.5,1.4,1.3,1.2,1.1,1.0];
%b=[5,4,3,2,1];
%b=[.12, .119, .118, .117, .116, .115, .114, .113, .112, .111, .110,
.109,
%.108, .107, .106, .105, .104, .103, .102, .101, .1];
%c=.12;
%a=1;
%c=5;

%a=.0016;
%c=.0270;
%b=.0016:.000635:.0270;

%lambda=.5;
alpha=(c-b)/(c-a);
gamma=1-alpha;

b_o=c-a;
b_oPrime=c-b;

d=c-b;
dPrime=b-a;

e=2.718;
gamma_one=.931161;
Xi=(pi*gamma_one)/(c/a-1);
```

```
%lambda=20; %as per p233 of Waveguide Handbook

%Section needs to be checked for dot product. Done. Checked for dot
product
%rules.
A=((1+alpha)./(1-alpha)).^(2*alpha)*((1+(1-
(b_o./(lambda*.5))^2)^.5)/(1-(1-(b_o./(lambda*.5))^2)^.5))-
((1+3*alpha.^2)./(1-alpha.^2));
APrime=((1+alpha)./(1-alpha)).^(2./alpha).*((1+(1-
(b_o./(lambda*.5)).^2).^.5)./(1-(1-
(b_oPrime./(lambda*.5)).^2).^.5))+((3+alpha.^2)./(1-alpha.^2));
C=((4*alpha)./(1-alpha.^2)).^2;


%variables calculated with dot product removed.
%A=((1+alpha)/(1-alpha))^(2*alpha)*((1+(1-
(b_o/(lambda*.5))^2)^.5)/(1-(1-(b_o/(lambda*.5))^2)^.5))-
((1+3*alpha^2)/(1-alpha^2));
%APrime=((1+alpha)/(1-alpha))^(2/alpha)*((1+(1-
(b_o/(lambda*.5))^2)^.5)/(1-(1-
(b_oPrime/(lambda*.5))^2)^.5))+((3+alpha^2)/(1-alpha^2));
%C=((4*alpha)/(1-alpha^2))^2;


A_one=(b./a).*(log(c/a)./((c/a)-1)).*(((c./b)-1)./log(c./b)).^2;

%A_two=(pi^2.*(a./b))./(gamma_one*(1-
((2*b_o)/(gamma_one*lambda))^2)^.5).*(((c/a)-
1)./((BESSELJ(0,Xi)^2)./((BESSELJ(0,Xi*(c/a))^2)-
1))).*((BESSELJ(0,Xi).*BESSELY(0,Xi.*b/a)-
BESSELY(0,Xi)*BESSELJ(0,Xi.*b/a))./((c./b)-1))^2-(1-
(2*b_o/lambda)^2)^-.5.*(2*b_o/(pi.*d)*sin(pi.*d/b_o)).^2;
A_twoa=(pi^2.*(a./b))/(gamma_one*(1-
((2*b_o)/(gamma_one*lambda))^2)^.5);
A_twob=(((c/a)-1)/((BESSELJ(0,Xi)^2)/((BESSELJ(0,Xi*(c/a)))^2)-1));
A_twoc=((BESSELJ(0,Xi)*BESSELY(0,(Xi/a).*b)-
BESSELY(0,Xi)*BESSELJ(0,(Xi/a).*b))./((c./b)-1)).^2;
A_twod=(1-(2.*b_o./lambda).^2).^-
.5.*(2.*b_o./(pi.*d).*sin(pi.*d./b_o)).^2;


%Old
%A_twoa=(pi^2*(a/b))/(gamma_one*(1-
((2*b_o)/(gamma_one*lambda))^2)^.5);
%A_twob=(((c/a)-1)/(((BESSELJ(0,Xi))^2)/(((BESSELJ(0,Xi*(c/a)))^2))-
1));
%A_twoc=((BESSELJ(0,Xi)*BESSELY(0,(Xi/a)*b)-
BESSELY(0,Xi)*BESSELJ(0,(Xi/a)*b))/((c/b)-1))^2;
%A_twod=(1-(2*b_o/lambda)^2)^-.5*(2*b_o/(pi*d)*sin(pi*d/b_o))^2;

%A_two=A_twoa*A_twob*A_twoc-A_twod;
A_two=A_twoa.*A_twob.*A_twoc-A_twod;
%plot(x,A_one);
```

```
%Axis([0 1 1 2.3])

%plot(x,A_two);
%Axis([0.01 1 0 .6])


%page 310, equation 2a

%BOverYo1=(2*b_o*A_one)/lambda*(2*log((1-
alpha^2)/(4*alpha))*((1+alpha)/(1-
alpha))^(.5*(alpha+1/alpha))+4*((A+APrime+2*C)/(A*APrime-
C^2))+.5*(b_o/lambda)^2*((1-
alpha)/(1+alpha))^(4*alpha)*(((5*alpha^2-1)/(1-
alpha^2))+4/3*(alpha^2*C/A))^2+A_two/2)

%with dot products
BOverYo1=(2*b_o.*A_one)./lambda.*(2*log((1-
alpha.^2)./(4*alpha)).*((1+alpha)./(1-
alpha)).^(.5*(alpha+1./alpha))+4*((A+APrime+2*C)./(A.*APrime-
C.^2))+.5*(b_o/lambda)^2*((1-
alpha)./(1+alpha)).^(4.*alpha).*(((5*alpha.^2-1)./(1-
alpha.^2))+4/3*(alpha.^2.*C./A)).^2+A_two/2);




%page 310, equation 2c

%BOverYo2=(2*b_o*A_one)/lambda*(gamma/2)^2*(4*log(2/gamma)/(1-
gamma)+2+17/2*(b_o/lambda)^2+A_two/2)

%with dot products
BOverYo2=(2*b_o.*A_one)/lambda.*(gamma/2).^2.*(4.*log(2./gamma)./(1-
gamma)+2+17/2*(b_o/lambda)^2+A_two/2);
%figure;
%plot(BOverYo2);

%figure;
%plot(alpha,BOverYo2, alpha, BOverYo1);


%A_two=(pi^2*(a./b))/(gamma_one*(1-
((2*b_o)/(gamma_one*lambda))^2)^.5)*(((c
%/a)-1)/((BESSELJ(0,Xi)^2)/((BESSELJ(0,Xi*(c/a))^2)-
1)))*((BESSELJ(0,Xi)*BESSELY(0,Xi.*b/a)-
BESSELY(0,Xi)*BESSELJ(0,Xi.*b/a))/((c./b)-1))^2-(1-
(2*b_o/lambda)^2)^-.5*(2*b_o/(pi.*d)*sin(pi.*d/b_o))^2;
```

VITA

James David Duvall

Candidate for the Degree of

Master of Science

Thesis: ISSUES PERTAINING TO DIELECTRIC ASSESSMENT OF SOIL MOISTURE IN A COAXIAL CELL

Major Field: Electrical Engineering

Biographical:

Education:
Completed the requirements for the Master of Science in Electrical Engineering at Oklahoma State University, Stillwater, Oklahoma in December, 2010.

Experience:

Professional Memberships:

Name: James Duvall Date of Degree: December, 2010

Institution: Oklahoma State University Location: Stillwater, Oklahoma

Title of Study: ISSUES PERTAINING TO DIELECTRIC ASSESSMENT OF SOIL MOISTURE IN A COAXIAL CELL

Pages in Study: 68 Candidate for the Degree of Master of Science

Major Field: Electrical Engineering

Scope and Method of Study: The study considered a pre-existing coaxial cell design and attempted to improve upon the accuracy of the coaxial cell as a measurement device. The cell was modeled with a revised transmission line model. Simulations were conducted using MatLab and were compared to data taken from an Agilent Vector Network Analyzer using Root Mean Square Error (RMSE) analysis to estimate the relative permittivity of samples contained in the coaxial cell's sample chamber.

Findings and Conclusions: It was found that while the new transmission line model was more rigorous in its representation of the coaxial cell, accuracy was still very limited. As a result, the coaxial cell should be redesigned to eliminate possible complications resulting from its current structure. A transmission line model may not be complex enough to properly represent the cell.

ADVISER'S APPROVAL: Dr. Charles Bunting